REVISITING THE CENSUS AND AGE OF THE BETA PICTORIS MOVING GROUP IN THE *GAIA* ERA

A THESIS SUBMITTED TO THE GRADUATE DIVISION OF THE
UNIVERSITY OF HAWAI'I AT MĀNOA IN PARTIAL FULFILLMENT
OF THE REQUIREMENTS FOR THE DEGREE OF

MASTER OF SCIENCE

IN

EARTH AND PLANETARY SCIENCES

DECEMBER 2022

By
Rena Aerey Lee

Thesis Committee:

Eric Gaidos, Chairperson
Gary Huss
Jennifer van Saders

Acknowledgements

A special thank you to Eric Gaidos, my research advisor and committee chair, for his support and guidance throughout my time at UH. It has been a pleasure, and I so greatly appreciate all he has done to push me forward and help me grow as a researcher and professional.

Thank you to my thesis committee members, Jen van Saders and Gary Huss, for all their helpful feedback and suggestions.

Thank you to Gregory Feiden and Jonathan Gagné, who have provided helpful feedback on this project as co-authors on the journal-submitted manuscript.

Thank you to the Fred Mason Bullard Fellowship foundation for financial support during my first year, and the National Science Foundation Graduate Research Fellowship Program during my final semester. It has been an honor to be acknowledged by these awards.

Thank you to Lily Shao for answering all my scattered questions and keeping me organized and afloat.

Thank you to Hope Ishii, my faculty mentor, for helpful conversations about life in academia, outside of my research.

Thank you to my dear friends here in Hawai'i who have made these past couple challenging years all the more enjoyable and uplifting. My survival in graduate school is largely owed to you all.

A very special thank you to my son (cat), Calcifer, who deserves esteemed acknowledgement for simply existing.

I could not be nearly the woman I am today without two outstanding role models in my life, my mom and sister. Thank you to my mom for providing me the foundation to pursue and achieve my goals. Thank you to Jane for always believing in me no matter those goals, and inspiring me to push myself in ways I never thought I could.

Abstract

Determining the precise ages of young (∼10 to few hundred Myr) kinematic ("moving") groups is important for placing star, protoplanetary disk, and planet observations on an evolutionary timeline. The nearby ∼25 Myr-old β Pictoris Moving Group (BPMG) is an important benchmark for studying stars and planetary systems at the end of the primordial disk phase. *Gaia* DR3 astrometry combined with ground-based observations and more sophisticated stellar models permit a systematic re-evaluation of its membership and age. We combined *Gaia* astrometry with previous and new radial velocities to evaluate moving-group membership in a Bayesian framework. To minimize the effect of unresolved stellar multiplicity on age estimates, we identified and excluded multi-star systems using *Gaia* astrometry, ground-based adaptive optics imaging, and multi-epoch radial velocities, as well as the literature identifications. We estimated age using isochrone and lithium-depletion-boundary fitting with models that account for the effect of magnetic activity and spots on young, rapidly rotating stars. We report an age of 33^{+9}_{-11} Myr to the BPMG based on isochrone fitting to the single-star and resolved-binary sample, which is older than, but within the uncertainties of, literature values.

Table of Contents

List of Tables

List of Figures

Chapter 1

Introduction

1.1 The Beta Pictoris Moving Group: A Young, Co-Eval Stellar Association

Associations of nearby, kinematically coherent, coeval stars, known as young moving groups (YMGs), are indispensable laboratories for studying early stellar and planetary evolution. Studies of YMG members have informed research on disk-dissipation and planet-formation timescales, early evolution of stellar evolution and magnetic activity, and the local stellar mass function (e.g., Kalas et al. 2004; Malo et al. 2014a; Binks & Jeffries 2017; Shkolnik et al. 2017). Accurately describing these evolutionary sequences relies on precise and accurate ages of these groups, e.g., by fitting of model isochrones or the lithium-depletion boundary to each group's stellar population (Bowler et al. 2019). Moreover, the ages of individual members (and their planets) can be robustly assigned to the ensemble age of the YMG. In recent years, the advent of all-sky photometric and astrometric surveys has enabled the identification, confirmation, and characterization of many new members of YMGs, as well as entirely new groups (Faherty et al. 2018; Gagné et al. 2018).

The β Pictoris Moving Group (BPMG), as the youngest, nearest (median distance $\sim$ 50 pc) YMG, affords some of the most detailed studies of pre-main sequence stars (pre-MS), including their intrinsically faintest (lowest and substellar-mass) members. Additionally, projected angular separations between binaries are larger, facilitating the identification and characterization of stellar and substellar companions. Its age, with recent isochronal estimates converging around 23 ± 3 Myr (Mamajek & Bell 2014), corresponds to an epoch immediately following the dissipation of protoplanetary disks and the initial phase in the evolution of fully-formed stars and planets. The BPMG's eponymous star, β Pictoris, hosts one of the first directly imaged debris disks (Lecavelier

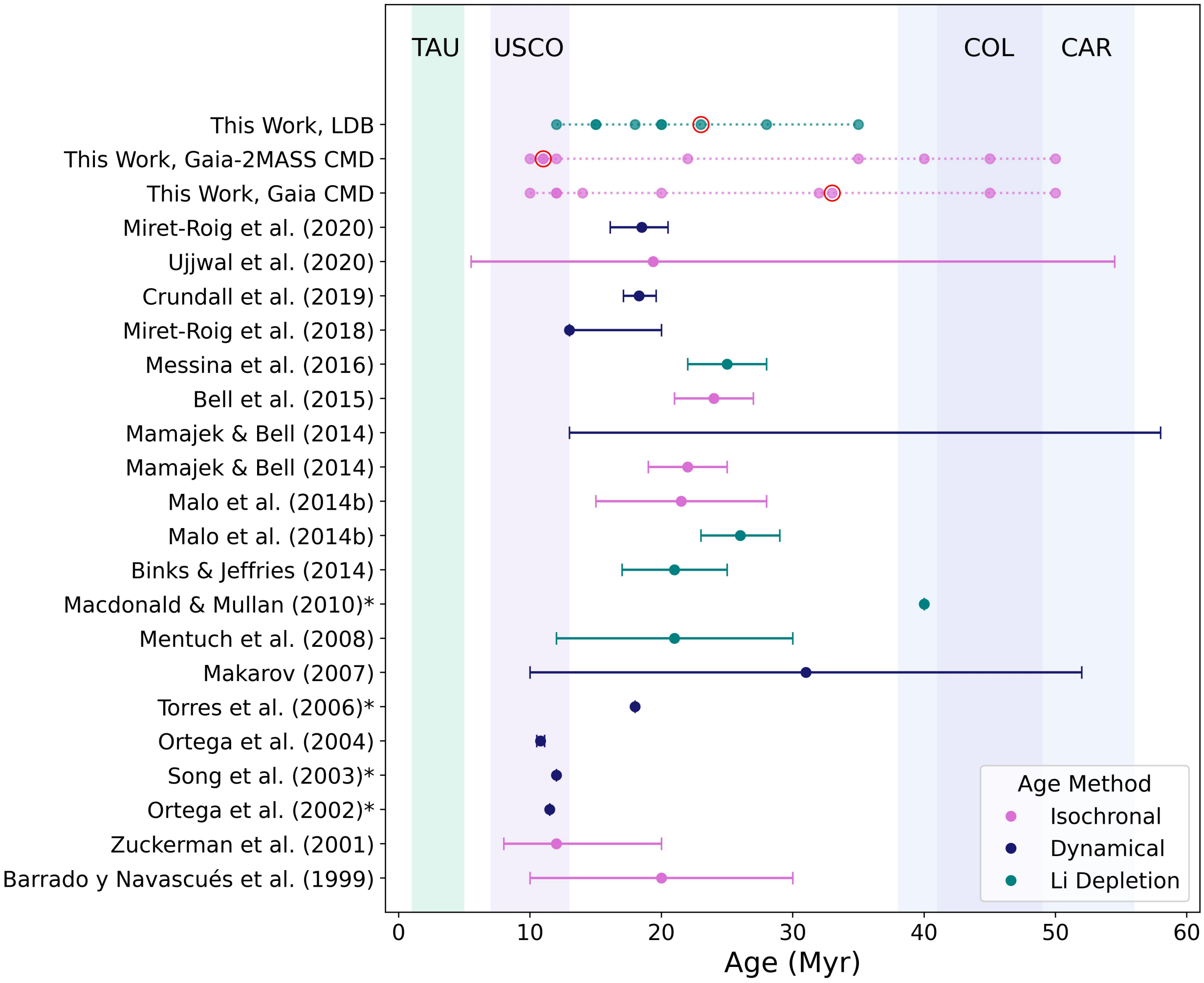

Figure 1.1 Literature-reported BPMG age estimates from Table 6 of Miret-Roig et al. (2020) (updated from Table 1 of Mamajek & Bell 2014), along with the isochronal and Li depletion ages from this study. Estimated ages of other young stellar associations Taurus (TAU), Upper Scorpius (USCO), Carina (CAR), and Columba (COL) have been plotted for comparison and context, gathered from Table 1 of Gagné & Faherty (2018) and references therein. The best-fit model age from each fit method in this work, the two color-magnitude diagrams (CMDs) and Li depletion boundary (LDB), are circled in red. Sources marked with an * do not report errors for their ages.

Des Etangs et al. 1993), as well as a rare directly imaged multi-planet system (Lagrange et al. 2020). Other BPMG members include 51 Eridani, hosting a directly imaged Jupiter analog (Macintosh et al. 2015), PSO J318.5-22, a free-floating planet (Liu et al. 2013), and AU Microscopii, hosting an edge-on debris disk and two transiting planets (Kalas et al. 2004; Plavchan et al. 2020; Cale et al. 2021).

1.2 Age-Dating BPMG: Precedents and Discrepancies

As seen in Fig. 1.1, the BPMG has been age-dated by fitting model isochrones to sequences in color-magnitude diagrams (CMDs), dynamical trace-back analyses, and lithium-depletion-boundary (LDB) model fitting. In this work, we utilize both isochrone and LDB models to assess the age of the BPMG.

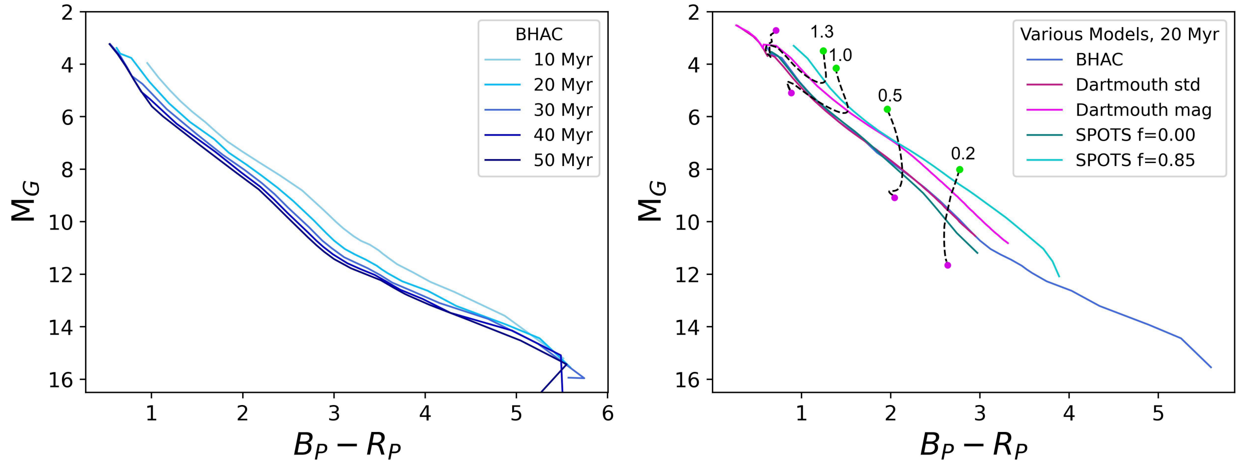

Figure 1.2 Various isochrone models plotted on a *Gaia G* vs. B_P-R_P CMD. The left panel shows isochrones from 10-50 Myr from Baraffe et al. (2015), while the right panel shows 20 Myr isochrones from the various models (Baraffe et al. 2015; Feiden 2016; Somers et al. 2020) used in this study (detailed in Sec. 3.1). For the SPOTS (Somers et al. 2020) models, we show the lowest (f=0.00) and highest (f=0.85) spot fraction models to exemplify the effect of increasing the spot fraction (refer to Sec. 1.2). The dashed black lines illustrate the evolution of individual stars of various masses (in solar masses, $M_\odot$) from 1 Myr (green dot) to 4 Gyr (magenta dot), from the SPOTS f=0.00 evolutionary tracks.

Isochrones are theoretical curves on a Hertszprung-Russell Diagram (HRD) or, the observational analog, a color-magnitude diagram (CMD; Fig. 1.2), identifying a co-eval population of stars at different masses. In a HRD or CMD, the horizontal axis represents temperature (roughly mass or color, as a proxy) while the vertical axis is the star's intrinsic brightness (i.e., absolute magnitude or luminosity). For main sequence (MS) and pre-MS stars, the higher mass, hotter stars will generally reside toward the upper left of the diagram, while the cooler, lower mass stars will be toward the lower right. Stellar evolutionary tracks follow a single star's evolution over time in luminosity (magnitude) vs. effective temperature (color) space (Kippenhahn et al. 2013). This is illustrated in the right-side panel of Fig. 1.2; the dashed lines show the evolution of single stars (0.2, 0.5, 1.0, 1.3 $M_\odot$) from 1 Myr (green points) to 4 Gyr (magenta points) (Somers et al. 2020). Connecting contemporary points across the different evolutionary tracks produces an isochrone. Isochrone models from 10-50 Myr from the (Baraffe et al. 2015) evolutionary models are plotted on a CMD in the left-side panel of Fig. 1.2. The CMD displays *Gaia* absolute magnitude (denoted as M_G) vs. color (B_P-R_P). The absolute magnitude is computed from the apparent magnitude and distance (parallax). The color is the difference in apparent magnitudes in two passbands, B_P and R_P, with the bluer magnitude preceding the redder by convention. From *Gaia*, B_P stands for blue photometer and R_P stands for red photometer. Even within this small age range, it is clear how stars of different masses (B_P-R_P, by proxy) evolve differently over time, especially at the younger (10-30 Myr) ages, where greater offsets in the isochrones are visible at different ranges of B_P-R_P. Generally, on the pre-MS, younger isochrones are above and toward the right of older ones.

For MS stars, the evolutionary models trace changes in luminosity and effective temperature due to surface gravity changes that result from nuclear fusion in stellar cores (Angus et al. 2019). Pre-MS evolution is distinct from MS evolution. For pre-MS stars, hydrogen burning has not yet begun; instead, the models trace the evolution of pre-MS stars fueled by gravitational contraction and deuterium fusion. Low-mass, pre-MS stars are fully convective, and the opacity in their interiors remains high until they reach temperatures hot enough to develop radiative cores (Kunitomo et al. 2017). Before this occurs, their luminosity is largely a function of gravity (and radius), so they decrease in luminosity as they contract. This is illustrated by their vertical, downward evolution on the CMD (known as Hayashi tracks) in Fig. 1.2. This evolution occurs on the Kelvin-Helmholtz (KH) timescale, and varies by mass. Once a radiative core develops and opacity drops, stars will move to the left of the diagram due to temperature increase, as is shown in the 1.0 and 1.3 $M_\odot$ tracks in Fig. 1.2. The MS is reached when a star begins hydrogen burning and reaches thermal equilibrium, where a star will spend ~80% of its lifetime. The lowest-mass stars (M dwarfs $\lessapprox$ 0.35 $M_{\odot}$) are fully convective even on the main sequence, thus their pre-MS evolution on the CMD remains almost entirely vertical.

As mentioned, for pre-MS stars such as the BPMG members, there are large differences in the evolutionary phases of stars at different masses. The KH timescale for stars increases inversely with mass, with the highest mass (> 8 $\mathrm{M}_{\odot}$) stars having KH radiative lifetimes shorter than their accretion time (Haemmerlé et al. 2017). Meanwhile, for the lower mass stars, the KH time is orders of magnitude longer than the accretion time (Stahler 1983). In other words, massive stars evolve much more rapidly than low mass stars. Thus, very high mass stars may already be evolving off the MS at the same age, even at young ages (Haemmerlé et al. 2019). Because of these contrasting behaviors, most evolutionary models do not span the very low to very high mass ranges.

A star's position on a CMD or HRD is sensitive to several physical mechanisms such as surface activity, multiplicity, or reddening/extinction. There are many evolutionary model grids and isochrones in the literature, tailored for different phases of evolution, mass ranges, and more complex stellar activity (e.g., Chabrier & Baraffe 1997; Yi et al. 2001; Baraffe et al. 2015; Dotter et al. 2008; Dotter 2016; Feiden 2016; Haemmerlé et al. 2019; Somers et al. 2020), and each have their own systematics and caveats. Isochrone model fitting is the most widely used method for estimating stellar ages, and relies on precise photometric data and distance measurements (via parallax) to estimate an age for a stellar association, in addition to an appropriate choice of models. As evident in the right-hand panel of Fig. 1.2, there are significant effects of including magnetism and surface spots in the models, because they account for the elevated luminosity resulting from magnetic activity. While all of the isochrones indicate a 20 Myr age, the Dartmouth magnetic and SPOTS high spot fraction (f=0.85) models appear younger (above and to the right) of their more standard counterparts (Dartmouth standard, BHAC, SPOTS f=0.00). For the models to converge on the same locus, we would need to increase the ages of the magnetic and spot fraction models, thus, the magnetic and spot fraction models would assign older ages to the same sequence of stars. The models utilized in this study are further described in Sec. 3.1.

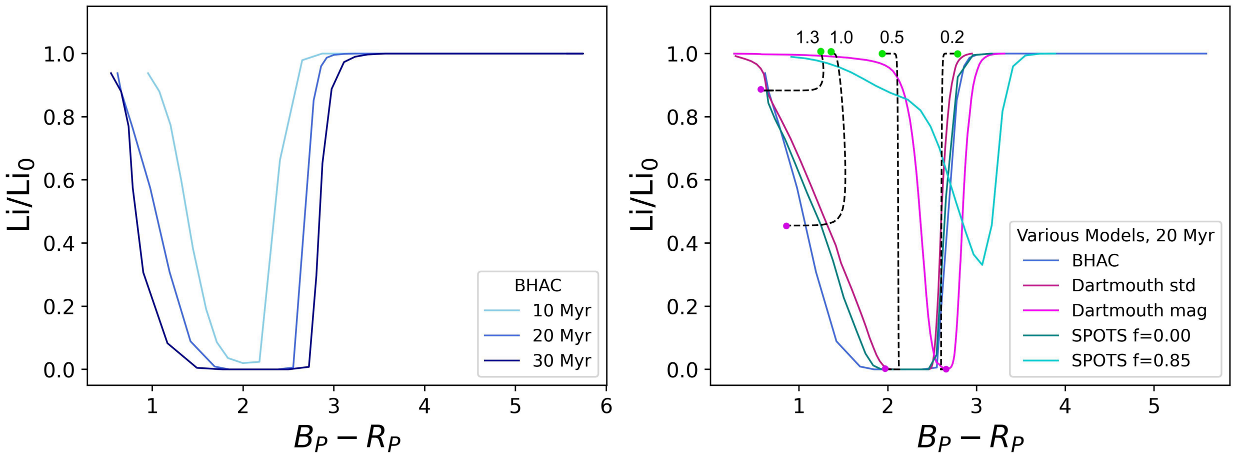

Figure 1.3 Various lithium depletion boundary (LDB) models, with abundances normalized to the primordial ISM value A(Li)=3.30 vs. $\mathrm{B_P}$-$\mathrm{R_P}$ color as a proxy for temperature. The left panel shows various age LDBs from Baraffe et al. (2015), while the right panel shows 20 Myr LDBs from the various models (Baraffe et al. 2015; Feiden 2016; Somers et al. 2020) used in this study (detailed in Sec. 3.1). For the SPOTS (Somers et al. 2020) models, we show the lowest (f=0.00) and highest (f=0.85) spot fraction models to exemplify the effect of increasing the spot fraction (refer to Sec. 1.2). The dashed black lines illustrate the evolution of individual stars of various masses (in solar masses, $M_\odot$) from 1 Myr (green dot) to 4 Gyr (magenta dot), from the SPOTS f=0.00 evolutionary tracks.

LDB fitting is another age-dating method commonly applied to stellar associations, comparing surface Li abundances by temperature (again, color as a proxy; Fig. 1.3). Measurements of surface Li abundances (equivalent width of the Li I 6708 Å line) in low-mass stars provide important information about their interior structures and nuclear ages (Palla et al. 2007). ^{7}Li is depleted by proton reactions at a threshold of about 2.5 $\times 10^6$ K (Burke et al. 2004). The LDB age estimate is the time it takes for internal temperatures to reach this threshold, and for lithium to be convected down into and destroyed in these regions. We show the LDB curves from 10-30 Myr from the (Baraffe et al. 2015) evolutionary models in Fig. 1.3 to illustrate how the boundary changes with time; generally the Li gap widens with age. At younger ages, the LDB (the right-hand side of the trough) is at higher masses (smaller $\mathrm{B_P}$-$\mathrm{R_P}$), because it takes more time for the lower-mass stars to reach the Li depletion temperature and for convective mixing to fully deplete Li. On the left-hand side of the boundary, photospheric temperatures are not high enough to destroy Li, and the onset of the radiative core structure leads to a halt in the Li depletion.

The LDB appears in the mass range of stars near the hydrogen-burning mass limit, which is a critical mass (∼0.1-0.3 $M_\odot$) at which a star cannot reach sufficient temperatures to undergo hydrogen burning, though degeneracy pressure provides sufficient support to sustain its surface luminosity. These are low mass stars reaching internal temperatures hot enough to burn lithium (Baraffe et al. 2017). This is a rapid process, as illustrated in Fig. 1.3 with the evolutionary tracks for 0.2, 0.5, 1.0, and 1.3 $M_\odot$ stars. For each track, there is a very steep drop-off in Li abundance, and for the lowest mass tracks (0.2-0.5 $M_\odot$), lithium is fully depleted very quickly. Meanwhile some Li remains in the more Sun-like stars and the very low-mass stars ($\lessapprox$ 0.7 $M_\odot$), which cannot reach the internal temperatures to burn lithium. The 20 Myr LDB from the various models used in this study (described in Sec. 3.1) are shown in 1.3 to illustrate how including magnetic and spot fraction effects change the LDB. Similar to the case of the isochrones, the 20 Myr Dartmouth magnetic and SPOTS f=0.00 models show younger LDBs (narrower) compared to the standard models.

For fully convective (<0.5 $M_\odot$) M dwarf stars, lithium is fully destroyed within ∼50 Myr (Bildsten et al. 1997). Mixing processes, such as overshooting, at the convective boundary have long posed a difficult obstacle in the evolutionary models (Shaviv & Salpeter 1973), and the convective activity is further complicated by effects from rotation (Baraffe et al. 2017). However, LDB fitting provides a useful comparison to isochrone fitting and is resistant to some of the systematics and limitations of photometry-reliant age estimates.

BPMG age estimates range between ∼10 and 50 Myr, with considerable variation in the uncertainties (Fig. 1.1, Mamajek & Bell 2014). The most-recent estimates cluster around ∼20-25 Myr, placing the BPMG at an intermediate stage between the Upper Scorpius star-forming region (10±3 Myr, Pecaut & Mamajek 2016), and the Carina YMG at ∼38-56 Myr old (Bell et al. 2015). According to the dynamical traceback studies (e.g., Crundall et al. 2019; Miret-Roig et al. 2020), the BPMG kinematics suggest a single star-forming event and origin, so it is unlikely that there is a real age spread among BPMG members.

Several effects can contribute to systematics and error in moving-group age estimates apparent in Fig. 1.1. Robust membership evaluation based on Galactic space motions requires precise parallaxes, proper motions, and radial velocities (RVs). Contamination by non-members from the field or other groups can also cause the cluster to appear older. Additionally, unresolved binarity can make members appear more luminous and hence younger than they actually are (Sullivan & Kraus 2021), affect the kinematics used for trace-back analysis, or influence the depletion of Li though the effect of a stellar companion on disk dissipation and stellar rotation (Somers & Pinsonneault 2015). Previous studies have highlighted the importance of identifying and excluding binary systems from group age analyses (e.g., Binks & Jeffries 2014; Alonso-Floriano et al. 2015). Recently, Miret-Roig et al. (2020) used *Gaia* DR2 astrometry and ground-based RVs to assess the BPMG age, identifying binaries based on the astrometry and RV variability.

An additional source of uncertainty in deriving ages from model comparisons comes from the high stellar rotation rates of the BPMG members. Due to their young age, these stars are rapidly rotating, and the surface spottedness and magnetic activity of pre-MS stars are observed to be enhanced compared to more quiescent MS stars (Morris 2020). Furthermore, it is not well known whether internal age gradients within stellar groups are physical. The mass-dependence of star formation timescales is not well defined, and multiple epochs of star formation may contribute to the scatter in group age estimates (Krumholz et al. 2019).

1.3 A Deeper Look with *Gaia* Space Observatory, New Evolutionary Models, and Resolved Multiplicity

An individual star's membership in a YMG is typically assessed by comparing its 6-d (3-d galactic position and 3-d space velocity) kinematics to that of the established group mean and dispersion. Previous BPMG membership studies have cataloged candidate members (i.e., Gagné & Faherty 2018) using incomplete astrometric (5-d; 3-d position and 2-d motion) information, followed by measurement of the 6th (RV) dimension to confirm membership (i.e., Schneider et al. 2019). Additionally, several studies have used RVs to identify binaries among BPMG members

(Alonso-Floriano et al. 2015; Messina et al. 2017; Miret-Roig et al. 2020). However, multi-epoch observations were often not available, thus precluding single-lined spectroscopic binaries from their identifications.

Gaia is a space observatory currently orbiting the Sun at LaGrangian point L2, creating the most precise and complete 3-d mapping of our galaxy (Gaia Collaboration et al. 2016). *Gaia* achieves this by scanning the sky continuously over many epochs, at different orientations, and very precisely timed. In its first data release (DR1), *Gaia* revolutionized the field of space astrometry by precisely measuring the parallaxes and proper motions of over 2 million objects (an order of magnitude more than *Hipparcos*, its predecessor mission). In each subsequent data release, *Gaia* has improved the completeness of its survey in addition to improving the precision of measurements, and supplying new measurements such as radial velocities (for a subset of targets). It provides more precise and homogeneous photometry and astrometry, in addition to RV measurements to improve membership validation and binary identification. The RV measurements from *Gaia* are yet incomplete, however, and are supplemented by other spectroscopic RV surveys such as RAVE (Malo et al. 2014a), surveying stars distributed in the Southern Hemisphere. *Gaia*'s latest data release, DR3, provides additional data, such as revised estimates of astrometric error (i.e. the Reduced Unit Weight Error, RUWE) to identify binaries not resolved by *Gaia* (Belokurov et al. 2020; Wood et al. 2021). Moreover, direct imaging searches for substellar companions to BPMG members have provided a wealth of archival high-angular-resolution adaptive optics (AO) images with which to resolve stellar companions at typical separations from ~100-1000 AU.

In addition to the new and improved astrometry and photometry, new, diverse evolutionary models are available to address some of the limitations of previously employed models (and assumptions) used to age-date BPMG. The spread between age estimates from different isochrone models can arise from a number of factors unique to each model, such as composition (hydrogen fraction X, helium fraction Y), metallicity (Z=[Fe/H]) or mixing length (Prada Moroni et al. 2016). Further, the complex activity of young, rapidly rotating stars complicates the photometry-reliant isochrone fitting (Morris 2020). This is especially true for later spectral types, since rotation and magnetic activity strongly influence the structure and convection of low-mass stars (Feiden

2016). To explore the model-dependent outcomes on age estimates, we compare isochronal fits from several suites of models, accounting for additional physical parameters such as magnetic pressure and surface spot fraction. The magnetic pressure and spot-fraction models are appropriate for the study of young, highly active BPMG stars still evolving on the pre-MS. The models accounting for the adjusted brightness of active stars would push the age estimate of BPMG older, though this is in conflict with the presence of debris and circumstellar disks observed in BPMG, which are typically thought to dissipate within the first tens of Myr.

In this work, we combined precision astrometry, photometry, and RVs from *Gaia* DR3 with ground-based RV measurements and AO imaging to assess and confirm moving group membership, identify and exclude close binaries, and distill a catalog of single-star members of the BPMG. We fit both isochrones and lithium depletion boundaries from new evolutionary models designed for spotted, magnetically active stars to precise, homogenous measurements of these stars to revisit the age of the BPMG, and consider the implications of the new, model-dependent ages. Further, we compare the lower-bound multiplicity fraction from this work with those of other young stellar associations.

Chapter 2

Methods

2.1 Catalog Construction

We obtained confirmed and candidate members of the BPMG from the Gagné et al. (2018) catalog, which analyzed all *Gaia* DR2 sources with precise parallaxes within the nearest 100 pc for YMG membership. We screened additional confirmed and candidate members from Binks & Jeffries (2014, 2016); Kiss et al. (2011); Lee & Song (2018); Messina et al. (2017); Shkolnik et al. (2017) leading to an initial catalog of 433 (assumed individual) stars. (We discuss a search for companions to these stars in Section 2.2.) This sample was cross-matched with *Gaia* DR3 (Gaia Collaboration et al. 2016, 2021), incorporating its updated and improved astrometry and photometry for 415 stars, and RVs for 99 stars. From DR2 to DR3, *Gaia* has improved parallax precision by ∼30%, proper motions by a factor of 2, and significantly reduced photometric systematics Gaia Collaboration et al. (2021).In addition to the *Gaia* data, RVs were gathered from RAVE DR6 (Guiglion et al. 2020), and previous RV surveys of low-mass stars and YMGs (i.e., Binks & Jeffries 2016; Malo et al. 2014a; Shkolnik et al. 2017; Terrien et al. 2015). RVs, either ground-based or from *Gaia*, were obtained for a total of 238 candidates.

We calculated probabilities of BPMG membership using `BANYAN` Σ, a multivariate Bayesian classifier. `BANYAN` Σ calculates UVW space velocities and XYZ galactic positions from coordinates, proper motions, parallaxes, RVs, and their errors, and compares these to the six-dimensional group means and standard deviations of the 27 nearest identified young moving groups (Gagné et al. 2018). For candidates with multi-epoch RV measurements, we used their median values in the `BANYAN` inputs. Based on the distribution of membership probabilities computed for candidates with complete kinematic data, we elected a threshold probability of 0.9; 148 of 238 with RV mesurements candidates were selected in this way. Separately, we identified 63 of the 195 candidates lacking RVs which would have membership probabilities >0.9 for an "optimal" RV that maximizes that probability and is plausible, i.e., the "optimal" RV, a statistical prediction assigned by `BANYAN`, was within the distribution of the measured RVs of confirmed members. These are high-priority targets for RV follow-up but are not further analyzed in this work.

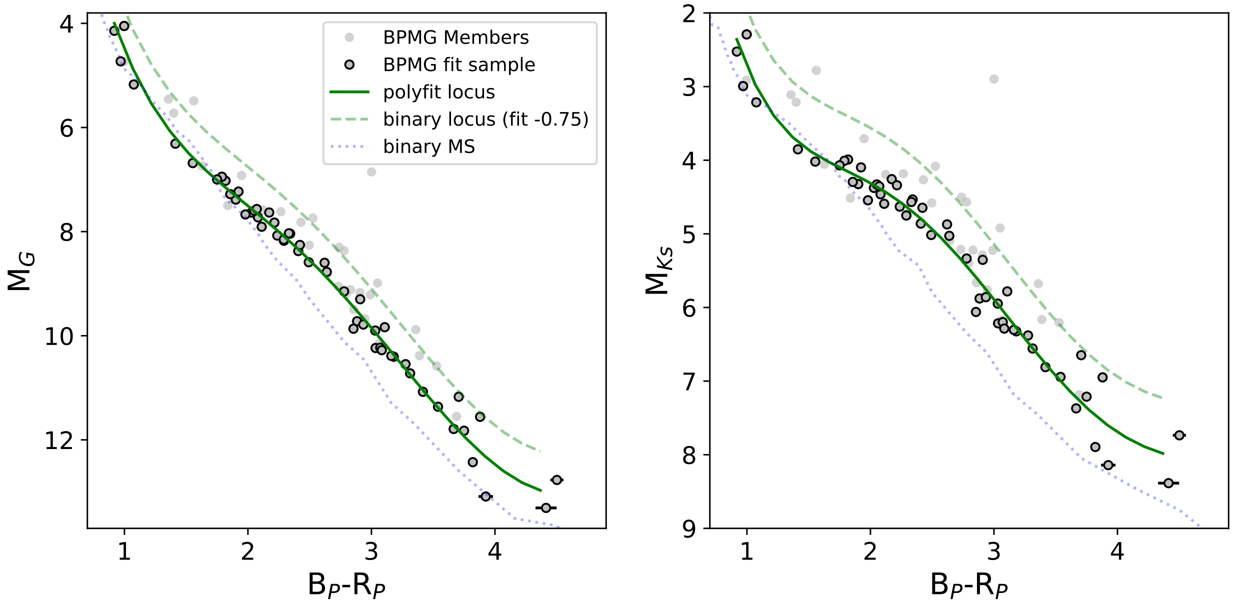

Figure 2.1 *Left:Gaia* color-magnitude diagram (CMD) of the BPMG sample. M_G is the absolute G magnitude, and B_P-P_P is the color, or the difference in magnitudes from the blue and red passbands on *Gaia*. *Right:* *Gaia*-2MASS CMD. M_Ks is the absolute Ks magnitude. The color is the same as in the left panel. All BPMG members confirmed in this study are shown as grey dots, while those passing the binary exclusion and photometric criteria are outlined in black. Only those outlined in black are used in the isochrone fitting described in Sec. 3.1. For both panels, we show the best-fit locus to the fit sample as a green line, and the approximate binary locus (-2.5log(2)≈0.75 mag, Sec. 2.2) in the dashed green line. Additionally, we show an approximate binary main-sequence locus from Mamajek & Bell (2014) as a blue dotted line.

We used the *Gaia* photometric color B_P-R_P as a proxy for temperature to plot the members in a CMD. In a *Gaia G* vs. B_P-R_P CMD (see Fig. 2.1 for binary-screened sample), we compared the P > 0.9 candidates against the empirical Mamajek & Bell (2014) MS to identify older MS interlopers contaminating the sample. We computed the minimum offset of each candidate from the MS model in color-magnitude space. We assigned a cutoff of offset<0.55 based on the distribution of this distance metric. A total of nine candidates with B_P-R_P > 2 were flagged as MS interlopers.

We still include those with B$_\mathrm{P}$-R$_\mathrm{P}$ $<$ 2, since hotter, bluer stars at this evolutionary phase may be arriving on the main sequence (Krumholz et al. 2019). Additionally, 5 photometrically outlying (over-luminous or over-reddened) candidates were removed from the membership sample with offset>1.03. Confirmed BPMG systems (single stars and unresolved and resolved binaries) are listed in Table 2.1. We cross-matched this BPMG sample with the 2-Micron All-Sky Survey (2MASS) catalog to obtain additional photometry in the infrared, and we corrected for extinction and reddening based on the Leike et al. (2020) 3-d ISM dust distribution using `dustmaps` (Green 2018). The mean value for reddening was E(B-V)=0.0005, and the mean extinction values were A(G) = 0.0003 and A(K$_s$) = 7.1×10^{-5}.

To account for inflated luminosity introduced by unresolved stellar companions, we corrected the K_s-band photometry of binaries that were resolved by *Gaia* but not resolved by 2MASS (noted in Table 2.1). We predicted 2MASS K_s magnitudes of each *Gaia*-resolved component using an empirical color-color relation between *Gaia* B_P-R_P and *Gaia G-2MASS* K_s based on the empirical main sequence of Mamajek & Bell (2014) and the *Gaia* DR3 B_P-R_P color and G magnitude of each component[1], and we then compared the predicted and the measured K_s mags. Based on the distribution of the differences, we flagged systems with a difference of 0.25 mag as significantly contaminated by a companion. Based on the contrast of the predicted K_s mags, we apportioned the measured K_s fluxes for each binary component accordingly, and recalculated the K_s mags for each component. This salvaged 9 systems to be used in the B_P-R_P vs. K_s CMD fitting in Sec. 3.1.

2.2 Binary Identification

We adopted resolved binary systems identified by Shkolnik et al. (2017) and Miret-Roig et al. (2020). We describe in this section additional resolved binary or multi-star systems in the *Gaia* DR3 astrometric catalog and AO imaging. To identify unresolved binaries, we examined *Gaia* DR3 Renormalized Unit Weight Error (RUWE), RV variability, and over-luminosity relative to the BPMG locus. In addition to addressing the effect of source confusion from unresolved binaries

---

[1] This color-color relation is based on main sequence stars and ignores metallicity effects but should be approximately correct for BPMG members.

in 2MASS and *Gaia* photometry, we identified additional BPMG members (stellar companions) to be included in the age-dating fit sample. Fig. 2.2 shows the approximate contrast-separation coverage of these methods. Along with the 50% AO detection efficiency contour described below, we show the *Gaia* 50% recovery contour for resolved binaries from Wood et al. (2021, and references therein), and the expected 50% recovery with RUWE based on Ziegler et al. (2018). Importantly, the AO imaging probes a region of parameter space inaccessible to *Gaia*.

Gaia DR3 resolved binaries: We identified sources within 30" with similar parallaxes and proper motions; this search radius corresponds to a reasonable binary separation of 1500 AU at the median distance of BPMG (∼50 pc). The probability that a nearby *Gaia* source is bound to a primary BPMG member is computed by:

$$P = d\mu * \exp\left[-\left(\frac{d\mu^2/2}{\sigma_\mu^2 + \mu_{orb}^2} + \frac{\delta\pi^2/2}{\sigma_\pi^2}\right)\right] \Bigg/ \frac{\sigma_\mu^2 + \mu_{orb}^2}{\sigma_\pi} \tag{2.1}$$

where $d\mu$ is the differences in the proper motions, σ_μ is the combined proper motion errors, $\mu_o rbit$ is the perturbation from orbit (negligible in this case), $\delta\pi$ is the difference in parallaxes, and σ_π is the parallax error of the potential secondary. We found 30 likely multi-star systems, 29 binaries and one triple system, from this computation, using a cutoff of P=0.98, based on the distribution of P. We could confirm 14 of these companions as BPMG members based on their astrometry, independent RVs, and `BANYAN`. The separations and contrasts of these 14 systems are shown in Fig. 2.2 as purple squares, labeled "Gaia Resolved."

Binary systems resolved in *Gaia* were included in subsequent analyses as they are not expected to have the same photometric contamination issues as unresolved binaries. However, the resolution is more limited in 2MASS; we recomputed individual photometry for components of binary systems resolved in Gaia but not 2MASS (final paragraph of Sec. 2.1) using an empirical color-color relation from (Mamajek & Bell 2014).

AO imaging: We collected archival AO images of confirmed BPMG members obtained with three instruments: NAOS+CONICA (NACO) on the ESO VLT UT1 (Lenzen et al. 2003; Rousset et al. 2003), NIRC2 on Keck (Service et al. 2016), and NIRI on Gemini-North (Hodapp et al.

2003) from the ESO, Keck Observatory, and Gemini Observatory archives, respectively. In each archive, we performed a cone search within 10” (the typical field of view) of the coordinates of each member. We recovered at least one AO image for 117 BPMG members, and we inspected each image for additional sources. We show in Fig. 2.2 the 16 AO-resolved binary components as pink triangles. An injection-and-recovery analysis was performed to assess the completeness and false positive rate of the visual inspection, by adding a simulated companion to randomly selected AO images containing a single (real) star. The point spread function of the target star was scaled and used for the simulated (fake) binary companion. The contrast of the simulated companion was randomly sampled from a uniform distribution in magnitude, and the separation was sampled from the Winters et al. (2019) orbital distribution of nearby M dwarf systems, assuming a distance of 50 pc. Separations were limited to 1.5 arcsec to focus on a region of the parameter space not resolved by *Gaia*, and because recovery should not change at larger separations. The results of the data injection recovery are shown in Fig. 2.2(right). We performed a kernel density estimation using `sklearn.neighbors.KernelDensity` on the detected and undetected simulated companions to establish a 50% detection efficiency contour in separation-contrast space.

Gaia RUWE: Gaia RUWE is a measure of astrometric error to a single-star fit analogous to reduced χ^2. Stars with RUWE > 1.4 are almost invariably unresolved binaries (Belokurov et al. 2020). Fitton et al. (2022) find that single stars hosting protoplanetary disks also exhibit elevated RUWE, but BPMG members are known to host only less substantial debris disks that have mostly accreted or dissipated (Lagrange et al. 2010). Twenty-nine members were identified as binaries based on RUWE.

Radial Velocity: Sources with ground-based RVs at more than one epoch or observation were assessed for binarity with a χ^2 difference test of the RV data. Based on the distribution of the reduced χ^2 values for stars with multiple RV epochs of observation, we chose a criterion of $\chi^2_\nu > 20$. If the binary sources were not resolved by *Gaia* or AO imaging, they were removed from the sample for age analyses. Seven such systems were not included in the CMD and lithium depletion boundary (LDB) fits. We show in Fig. 2.2 an estimated RV detection limit contour based on the separations and contrasts of the resolved BPMG binaries and the average RV amplitude from members with

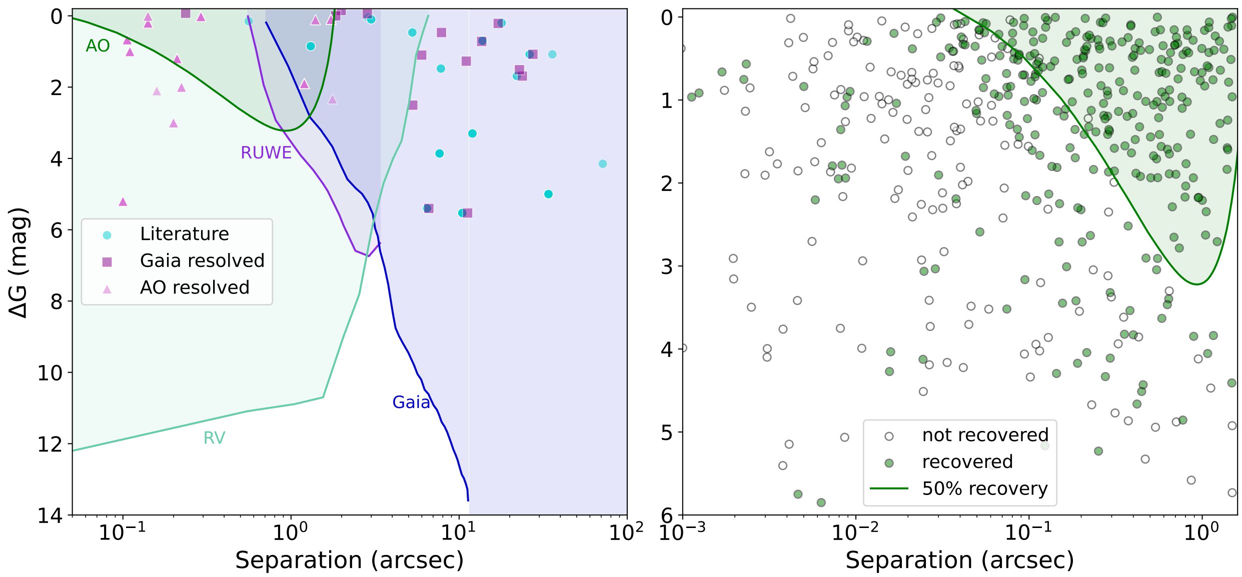

Figure 2.2 *Left*: Separation vs. contrast for binary components in the BPMG primary sample from the present *Gaia* cone search astrometry comparison and AO image inspection, as well as literature-reported binaries. Unresolved spectroscopic, RV, and RUWE-identified binaries are not included. We show an empirical 50% recovery contour of RUWE binaries from Wood et al. (2021), along with 50% recovery contour for *Gaia*-resolved binaries from Ziegler et al. (2018) and the 50% recovery for AO from our injection-and-recovery tests. The estimated RV detection limit is shown in light green. *Right*: Results of the AO injection-and-recovery analysis. Simulated binaries that were not detected by eye (false negatives) are plotted as open points, and successfully identified simulated binaries are plotted as green points. The contour represents a 50% detection efficiency. The simulated binaries stayed within 1.5”, since recovery is not expected to change at larger separations.

multi-epoch RVs. We computed the expected separations and contrasts of unresolved systems assuming a typical primary mass of 0.3 $M_\odot$ and maximum separation of 1000 AU. Additionally, p-values for RV variability are included for many sufficiently bright stars in *Gaia* DR3 (Chance et al. 2022) and 14 sources for which $p < 0.01$ were flagged as binary systems.

Photometry: Binaries unresolved by *Gaia* were assumed to be equal-brightness, i.e. the most probable configuration (Duchêne & Kraus 2013), with equal partitioning of the flux. From the conversion of flux to magnitude, this translates to a factor of -2.5*log(2)≈0.75 mag. We estimated the equal mass binary locus of BPMG by shifting the BPMG polyfit locus (described in Sec. 2.1) by +0.75 mag. We then examined the offsets of BPMG members from the binary locus. We quantified this offset by the difference in the binary locus *Gaia* G mag and the observed, ΔM_G, and removed 18 likely photometric binaries from the age-dating fit sample based on a cut-off range of $0.7 < \Delta M_G < 0.75$ mag, which was assessed from the distribution of all offsets computed. The unresolved (RUWE, RV, and photometric) binaries are excluded from the isochrone fitting. Since they are not resolved, they are not given in Fig. 2.2(left), though we provide approximate detection limits for these methods. The final sample is shown in a *Gaia* absolute G mag (M_G) vs. B_P-R_P color CMD in Fig. 2.1.

Table 2.1 Confirmed BPMG members in this study.

Gaia DR3 ID	2MASS ID	Common Name	RA	DEC	Plx (mas)	G	BP-RP	Binary Flag	Sep (as)
2315841869173294208	00275035-3233238	GJ 2006 B	00:27:50.35	-32:33:24.13	28.59	11.92	2.80	R	17.890
2315849737553379840	00281434-3227556	GR* 9	00:28:14.35	-32:27:55.62	28.56	13.44	3.31	N	
2357025657739386624	00482667-1847204		00:48:26.67	-18:47:20.42	19.42	13.94	3.16	N	
2581708281894978176	00501752+0837341		00:50:17.51	+08:37:34.20	6.31	12.85	3.00	U	
2788357364871430400	01025097+1856543		01:02:50.99	+18:56:54.16	26.19	12.58	2.95	U	
2477870708709917568	01351393-0712517	Barta 161 12	01:35:13.92	-07:12:51.46	26.82	11.97	2.83	U	
73034991155555456	02175601+1225266		02:17:56.02	+12:25:26.42	15.90	12.81	2.64	U	
87555176071871744	02241739+2031513		02:24:17.40	+20:31:51.42	14.13	16.04	3.67	N	
132363027978672000	02272804+3058405	AG Tri B	02:27:28.06	+30:58:40.36	24.43	11.43	2.41	R	22.050
132362959259196032	02272924+3058246	AG Tri A	02:27:29.25	+30:58:24.60	24.42	9.74	1.55	U	
22338644598132096	02442137+1057411	MCC 401	02:44:21.37	+10:57:41.07	20.78	10.33	1.95	R	0.223
5177677603263978880	02450826-0708120		02:45:08.27	-07:08:12.09	14.66	14.00	3.11	N	
5183875103632956032	02495639-0557352		02:49:56.38	-05:57:35.43	15.09	15.66	3.88	U	
68012529415816832	03350208+2342356	EPIC 211046195	03:35:02.09	+23:42:35.41	19.72	16.30	4.50	N	
244734765608363136	03393700+4531160		03:39:37.01	+45:31:15.97	24.82	12.89	2.85	U	
66245408072670336	03573393+2445106	StKM 1-433	03:57:33.93	+24:45:10.64	14.55	11.86	1.98	N	
3205094369407459456	04373746-0229282	GJ 3305	04:37:37.46	-02:29:28.95	36.01	9.80	2.12	R	0.235
175329120598595200	04435686+3723033	PM J04439+3723W	04:43:56.87	+37:23:03.36	14.01	12.31	2.34	R	7.650
3231945508509506176	04593483+0147007	V1005 Ori	04:59:34.83	+01:47:00.67	40.99	9.32	1.90	N	
4764027962957023104	05004714-5715255	CD-57 1054	05:00:47.13	-57:15:25.45	37.21	9.38	1.92	N	
3228854506445679616	05015665+0108429		05:01:56.65	+01:08:42.90	39.54	11.51	2.86	U	
3238965099979863296	05061292+0439272		05:06:12.93	+04:39:27.18	36.19	11.99	2.93	N	
2962658549474035584	05064991-2135091	BD-21 1074 A	05:06:49.50	-21:35:04.30	50.43	9.56	2.24	R	7.790
2901786974419551488	05294468-3239141	SCR J0529-3239	05:29:44.69	-32:39:14.30	33.60	12.27	3.03	N	
3216729573251961856	05320450-0305291	V* V1311 Ori	05:32:04.50	-03:05:29.40	27.22	10.44	2.27	R	0.159
3216922640621225088	05335981-0221325		05:33:59.82	-02:21:32.38	29.12	11.27	2.49	U	
2899492637251200512	06131330-2742054		06:13:13.32	-27:42:05.57	29.62	10.94	2.74	R	0.110
5266270443442455040	06182824-7202416	AO Men	06:18:28.21	-72:02:41.45	25.57	9.27	1.41	N	
5412403269717562240	09462782-4457408		09:46:27.82	-44:57:40.85	21.44	14.52	3.71	N	
5355751581627180288	10172689-5354265	TWA 22 A	10:17:26.89	-53:54:26.39	50.52	12.06	3.53	R	0.106
5849837854861497856	14423039-6458305	* alf Cir	14:42:30.42	-64:58:30.49	60.99	3.17	0.54	U	

The ‘Binary Flag’ column reflects whether the system was identified as a binary in this study. N = not binary, U = unresolved binary, and R = resolved binary. For resolved binaries, the angular separation is listed in the ’Sep’ column in arcseconds. This table is continued in the following pages.

Table 2.1, continued.

Gaia DR3 ID	2MASS ID	Common Name	RA	DEC	Plx (mas)	G	BP-RP	Binary Flag	Sep (as)
5882581895192805632	15385679-5742190	V343 Nor BC	15:38:56.78	-57:42:18.95	25.44	13.21	3.03	R	10.450
5882581895219921024	15385757-5742273	V343 Nor A	15:38:57.56	-57:42:27.35	25.83	7.68	1.00	U	
5935776714456619008	16572029-5343316		16:57:20.27	-53:43:31.58	19.69	11.35	2.43	R	0.100
5963633872326630272	17024014-4521587	UCAC2 12510535	17:02:40.16	-45:21:58.72	31.30	10.70	2.29	N	
4107812485571331328	17150362-2749397	CD-27 11535	17:15:03.61	-27:49:39.74	12.00	10.09	1.56	R	0.141
5811866422581688320	17172550-6657039	HD 155555 B	17:17:25.51	-66:57:03.73	32.95	6.46	1.00	U	
5811866422581688320	17172550-6657039	HD 155555 A	17:17:25.51	-66:57:03.73	32.95	6.46	1.00	U	
5811866358170877184	17173128-6657055	HD 155555 C	17:17:31.29	-66:57:05.47	32.88	11.47	2.73	R	34.010
5924485966955008896	17295506-5415487	CD-54 7336	17:29:55.08	-54:15:48.65	14.79	9.32	1.08	N	
4067828843907821824	17520173-2357571	UCAC4 331-124196	17:52:01.74	-23:57:57.22	15.67	11.85	2.21	N	
4050178830427649024	18041617-3018280		18:04:16.18	-30:18:27.96	18.15	11.74	2.33	N	
6648834361774839040	18055491-5704307	UCAC3 66-407600	18:05:54.92	-57:04:30.74	17.71	12.36	2.62	N	
6414282147589248000	18090694-7613239		18:09:06.93	-76:13:23.89	36.66	13.26	3.42	N	
6653162456161626368	18092970-5430532		18:09:29.71	-54:30:53.27	25.67	13.34	3.39	U	
4045698732855626624	18142207-3246100		18:14:22.07	-32:46:10.13	13.92	11.91	2.17	R	1.200
6706431763001502848	18151564-4927472		18:15:15.64	-49:27:47.30	16.13	11.70	2.53	U	
4051081838710783232	18195221-2916327	HD 168210	18:19:52.21	-29:16:32.82	12.43	8.67	0.92	U	
6705107126367751168	18265401-4807022	HD 169405	18:26:54.01	-48:07:02.06	12.20	5.22	1.03	U	
6723183789033085824	18283208-4129081	TYC 7909-2501-1	18:28:32.09	-41:29:08.36	14.96	10.86	1.63	U	
6649786646225001984	18420483-5554126		18:42:04.84	-55:54:12.74	19.36	13.84	3.08	N	
6649788119394186112	18420694-5554254		18:42:06.96	-55:54:25.58	19.44	12.33	2.64	N	
6728469996119674112	18430597-4058047		18:43:05.97	-40:58:04.78	17.10	12.10	2.50	U	
6650036304082834560	18443965-5506502		18:44:39.66	-55:06:50.09	11.02	10.24	1.36	U	
6631685008336771072	18465255-6210366	Smethells 20	18:46:52.55	-62:10:36.61	19.72	11.13	2.05	N	
4071532308311834496	18471351-2808558		18:47:13.51	-28:08:55.86	16.69	15.25	3.54	N	
6736232346363422336	18504448-3147472	CD-31 16041	18:50:44.48	-31:47:47.38	20.22	10.49	1.82	N	
6655168686921108864	18530587-5010499	HIP 92680	18:53:05.87	-50:10:49.90	21.16	8.10	0.97	N	
4088823159447848064	19082195-1603249		19:08:21.96	-16:03:24.82	14.35	15.77	3.69	U	
6764026419748892160	19114467-2604085	CD-26 13904	19:11:44.67	-26:04:08.53	14.77	9.88	1.40	R	0.210
6663346029775435264	19233820-4606316		19:23:38.21	-46:06:31.64	14.03	11.21	1.79	N	
6742986538895222144	19243494-3442392		19:24:34.95	-34:42:39.37	19.40	12.77	2.99	U	
6643851448094862592	19260075-5331269		19:26:00.75	-53:31:26.97	20.94	12.57	2.91	U	

Table 2.1, continued.

Gaia DR3 ID	2MASS ID	Common Name	RA	DEC	Plx (mas)	G	BP-RP	Binary Flag	Sep (as)
6764421281858414208	19300396-2939322		19:30:03.96	-29:39:32.45	16.60	13.20	2.91	N	
6754492966739292928	19481651-2720319		19:48:16.52	-27:20:31.94	15.47	12.21	2.29	N	
6754492932379552896	19481703-2720334		19:48:17.05	-27:20:33.50	15.34	17.16	3.93	N	
6747467431032539008	19560294-3207186		19:56:02.94	-32:07:18.66	19.54	11.91	2.78	R	26.310
6747467224874108288	19560438-3207376	TYC 7443-1102-1	19:56:04.37	-32:07:37.67	19.49	10.83	1.86	N	
6747106443324127488	20013718-3313139		20:01:37.17	-33:13:14.01	16.68	11.46	2.07	N	
6700649538727351040	20055640-3216591		20:05:56.41	-32:16:59.19	20.18	11.20	2.08	N	
6850555648387276544	20083784-2545256		20:08:37.85	-25:45:25.71	17.85	14.15	3.18	N	
6800238044930953600	20333759-2556521		20:33:37.60	-25:56:52.12	22.90	13.08	3.36	U	
6794047652729201024	20450949-3120266	AU Mic	20:45:09.53	-31:20:27.24	102.94	7.84	2.11	N	
6833291426043854976	21100461-1920302		21:10:04.61	-19:20:30.44	29.77	11.62	3.05	R	0.141
6833292181958100224	21100535-1919573		21:10:05.36	-19:19:57.61	30.90	10.81	2.42	N	
6801191424589717888	21103096-2710513	BRG 32B	21:10:30.97	-27:10:51.53	24.84	14.85	3.75	N	
6801191355870240768	21103147-2710578		21:10:31.48	-27:10:58.01	24.76	13.58	3.28	N	
6835588645136005504	21200779-1645475		21:20:07.81	-16:45:47.80	20.72	13.14	2.88	N	
6400160947954197888	21212873-6655063		21:21:28.72	-66:55:06.27	31.70	9.99	1.84	U	
2727844441062478464	22085034+1144131		22:08:50.34	+11:44:13.22	26.75	13.02	3.06	U	
6608255235884536320	22334687-2950101		22:33:46.89	-29:50:10.22	19.19	16.89	4.41	N	
6382640367603744128	22424896-7142211		22:42:48.93	-71:42:21.20	27.23	9.82	1.75	N	
6603693881832177792	22445794-3315015	HIP 112312 A	22:44:57.96	-33:15:01.74	47.92	10.74	2.78	R	35.880
6603693808817829760	22450004-3315258	HIP 112312 B	22:45:00.06	-33:15:26.09	48.00	11.82	3.07	N	
2433191886212246784	23323085-1215513	BD-13 6424	23:32:30.86	-12:15:51.46	36.43	9.83	2.03	N	
2324205785406060928	23355015-3401477		23:35:50.17	-34:01:47.78	26.76	15.29	3.82	N	

Chapter 3

Model Fitting for Age Determination

3.1 Color-Magnitude Diagram Isochrone Fitting

CMD isochrone fitting was described in Sec. 1.2. We estimated the age of the BPMG by fitting isochrones from different models to the color-absolute magnitude diagram of confirmed members. We excluded binaries that are not resolved by *Gaia*, leaving 107 single stars and 46 components of resolved binaries. The *Gaia* G vs. $\mathrm{B_P}$-$\mathrm{R_P}$ and 2MASS Ks vs. $\mathrm{B_P}$-$\mathrm{R_P}$ color magnitude diagrams of these stars are plotted in Fig. 4.2 along with the isochrone fits.

We compared these observations with the pre-main sequence models of Baraffe et al. (2015), Dartmouth standard and magnetic models (Feiden 2016), and the SPOTS models of Somers et al. (2020). The Baraffe et al. (2015) models (hereafter, BHAC) are calibrated for pre-MS and MS low-mass stars. The evolutionary calculations are based on standard input physics of stellar interiors (Chabrier & Baraffe 1997), but with updated atmosphere models compared to the predecessory evolutionary models of Baraffe et al. (1998). While the BHAC models are calibrated for pre-MS stars, they do not account for the effects of stronger magnetic fields occurring at the surfaces of young, rapidly rotating stars. We used the `scipy.interpolate.interp1d` function to produce a finer age model grid (spaced by 1 Myr) than is provided in Baraffe et al. (2015) to better compare with the Dartmouth and SPOTS model grids. We interpolated the model *Gaia* and 2MASS magnitudes based on the supplied model masses, magnitudes, and ages.

Dartmouth stellar evolution models are suitable for modeling low-mass main sequence (Dotter et al. 2008) and pre-MS stars (Feiden 2016), with or without effects of stellar magnetic fields (Feiden & Chaboyer 2012; Feiden 2016). These models were used to age-date BPMG in Malo et al. (2014b). Their interior structure and evolution calculations adopt standard input physics (e.g., solar-calibrated mixing length, general ideal gas equation-of-state, PHOENIX (Hauschildt et al. 1999) model atmospheres) comparable to other modern low-mass stellar models (e.g., BHAC; Dotter et al. 2008) with updates to improve the accuracy of model predictions for very-low-mass stars and the pre-main-sequence phase of stellar evolution (e.g., Malo et al. 2014b; Feiden et al. 2015). Models including magnetic fields account for the impact of magnetism on the gas equation of state and on the efficiency of thermal convection (Feiden & Chaboyer 2012; Feiden 2016). Surface magnetic field strengths are assumed to be in pressure equipartition with the gas near the stellar photosphere (Feiden (2016)). The model grid assumes solar metallicity (appropriate for the BPMG) and solar composition (Grevesse et al. 2007) and includes individual mass tracks with $0.1 \leq M/M_{\odot} \leq 2.0$, and isochrones with ages from 1 Myr – 10 Gyr. Synthetic *Gaia* photometry is calculated using synthetic spectra from MARCS model atmospheres (Gustafsson et al. 2008), 2MASS JHK passbands (Skrutskie et al. 2006), and revised *Gaia* DR2 passbands (Evans et al. 2018) assuming the total extinction (A_V) is zero.

The SPOTS evolutionary models (Somers et al. 2020) address the distorting effects of activity and surface spots on the structure of magnetically active stars. The model grid includes evolution tracks and isochrones for 0.1 – 1.3 $\mathrm{M}_{\odot}$ stars with discrete surface spot coverage fractions of $f=$ 0.0, 0.17, 0.34, 0.51, 0.68, and 0.85. The SPOTS isochrones are empirically calibrated from the color transformations of Pecaut & Mamajek (2013). However, *Gaia* magnitudes and colors are not provided for objects redder than B_{P}-R_{P} $\sim$2.5 for models with spot fraction > 0. We extend the fits down to B_{P}-R_{P}=3.0 for the spot fraction > 0 isochrones using the model luminosity, gravity, mass, and dual-temperature regime (for hot and cool surface regions) to obtain bolometric corrections (and hence absolute magnitudes) for *Gaia* G, B_P, and R_P and 2MASS Ks magnitudes from the YBC database (Chen et al. 2019), assuming A_V=0 and solar metallicity. The $\mathrm{B_P}$-$\mathrm{R_P}$ color were generated by taking the difference in absolute $\mathrm{B_P}$ and $\mathrm{R_P}$ magnitudes.

We modified the spot fractions, which are specified in terms of surface area, to fractions in luminosity using the formulation

$$f' = \frac{f}{f + (1-f)(T_{hot}/T_{cool})^4}. \tag{3.1}$$

The two model temperatures, T_{hot} and T_{cool} from SPOTS were used to separately compute magnitudes and relative fluxes for hot and cool surface regions, and an average flux was computed based on our modified spot fractions. Objects redder than $\mathrm{B_P}$-$\mathrm{R_P}$=3 are still included in the fits.

We used the τ^2 isochrone fitting metric (Naylor & Jeffries 2006), a form of maximum-likelihood two-dimensional fitting in color-magnitude space. τ^2 behaves essentially as a χ^2 statistic, with an added dependence on the model density of stars in color-magnitude space (ρ in Eq. 5 of Naylor & Jeffries (2006)). We show in Fig. 4.2 the results of our isochrone fitting analysis for each of the nine models (BHAC, Dartmouth standard, Dartmouth magnetic, and each of the six spot fraction models from SPOTS), in *Gaia* $\mathrm{B_P}$-$\mathrm{R_P}$ vs. M_G and M_{Ks} CMDs. To better visualize the model performance on the CMD, we also show the difference in absolute magnitude vs. $\mathrm{B_P}$-$\mathrm{R_P}$ for each model from a best-fit curve to the main BPMG locus, which was computed using the `numpy.poly1d` and `numpy.polyfit` functions (see Fig. 2.1 for a clean look at the sample and polyfit curve). We supply in Table 4.1 the age results and τ^2 values from each of the fits.

3.2 Lithium Depletion Boundary Analysis

LDB model fitting was described in Sec. 1.2. We compared the abundance of lithium vs. effective temperature to model predictions as an independent constraint on the age of the BPMG. Li 6708Å equivalent width (EW) measurements and upper limits were gathered from the literature (Bowler et al. 2019; Mentuch et al. 2008; Messina et al. 2016; Zuckerman et al. 2001) for single BPMG members. For this analysis, we chose to exclude binary systems due to confusion in deriving accurate abundances for each binary component. Additionally, the presence of a companion may affect rotation rates and lead to lithium depletion on faster timescales than in single star systems. The EW measurements were converted to abundances based on the curves of growth of Palla et al. (2007) in the $\mathrm{T_{eff}}$ range 3100 –3600 K and Soderblom et al. (1993) in the $\mathrm{T_{eff}}$ range 4000 – 6500 K. We normalized the Li abundances to the ISM value of A(Li) = 3.30 based on meteoritic abundances, a proxy for Li in the protosolar value (Asplund et al. 2009). The typical abundance uncertainty was computed by interpolating the typical EW error over model temperature. We show the converted

Li abundances as a function of *Gaia* $\mathrm{B_P}$-$\mathrm{R_P}$, a proxy for effective temperature, in Fig. 4.3, along with the model Li abundances from each of the nine models. For each of the models, we identified the best-fit $\mathrm{Li/Li_0}$ vs. $\mathrm{B_P}$-$\mathrm{R_P}$ curves by minimum χ^2 fit. A description of the LDB is given in Sec.1.1.

Chapter 4

Results

4.1 Membership and Binarity Census

The BPMG catalog is presented in Table 2.1. Binary systems are noted in the ‘Binary Flag’ column. Resolved systems for which we re-computed the 2MASS *Ks* magnitudes are marked with an * in the ‘*Ks* mag’ column. This is the most kinematically complete BPMG census available based on the latest *Gaia* astrometry and and extensive literature search of RVs. An extended machine-readable data table is available upon request.

To summarize, from our membership and binary identification analyses we recovered 238 candidates compiled from the literature had sufficient kinematic data to be analyzed in `BANYAN`. 148 candidates advanced with a probability of BPMG membership > 0.9, and 9 of the 148 candidates were identified as MS interlopers and removed from the membership census, leaving 139 confirmed members. 5 members were excluded from subsequent analyses due to problematic photometry whose cause was unclear. 15 members were already identified in the literature as binaries. 30 systems were identified as resolved binary systems using *Gaia* astrometry in a Bayesian framework; 14 new companions were independently confirmed in `BANYAN`, making the total membership count 153. 16 binary companions were resolved in AO images; 4 were identified in the *Gaia* search. 47 total systems were excluded from isochronal fits due to unresolved binarity; 29 from the *Gaia* RUWE criterion, 21 from RV variability, and 18 photometric binaries; there is some overlap between methods. We present a BPMG catalog of 153 systems, including 42 resolved binaries, 47 unresolved binaries, and 64 single stars. We report a multiplicity fraction of ∼42%, the fraction of binary to single systems in this sample, consistent with the literature pre-main sequence stars between star-forming regions (∼50-58%, Ghez et al. (1997)) and main-sequence M dwarfs (up to ∼41%, Shan et al. (2017); Zúñiga-Fernández et al. (2021)). We show a comparison of our results to other YMGs in Fig. 4.1, adapted from Shan et al. (2017). In Shan et al. (2017), they report multiplicity fractions from AO imaging, astrometry, and spectroscopy. Age estimates are based on BANYAN and SACY membership catalogs. Our result is plotted in black to distinguish from the literature results (Jaehnig et al. 2017; Shan et al. 2017; Kounkel et al. 2019; Zúñiga-Fernández et al. 2021), and clearly is in agreement with the majority of similarly-aged YMGs.

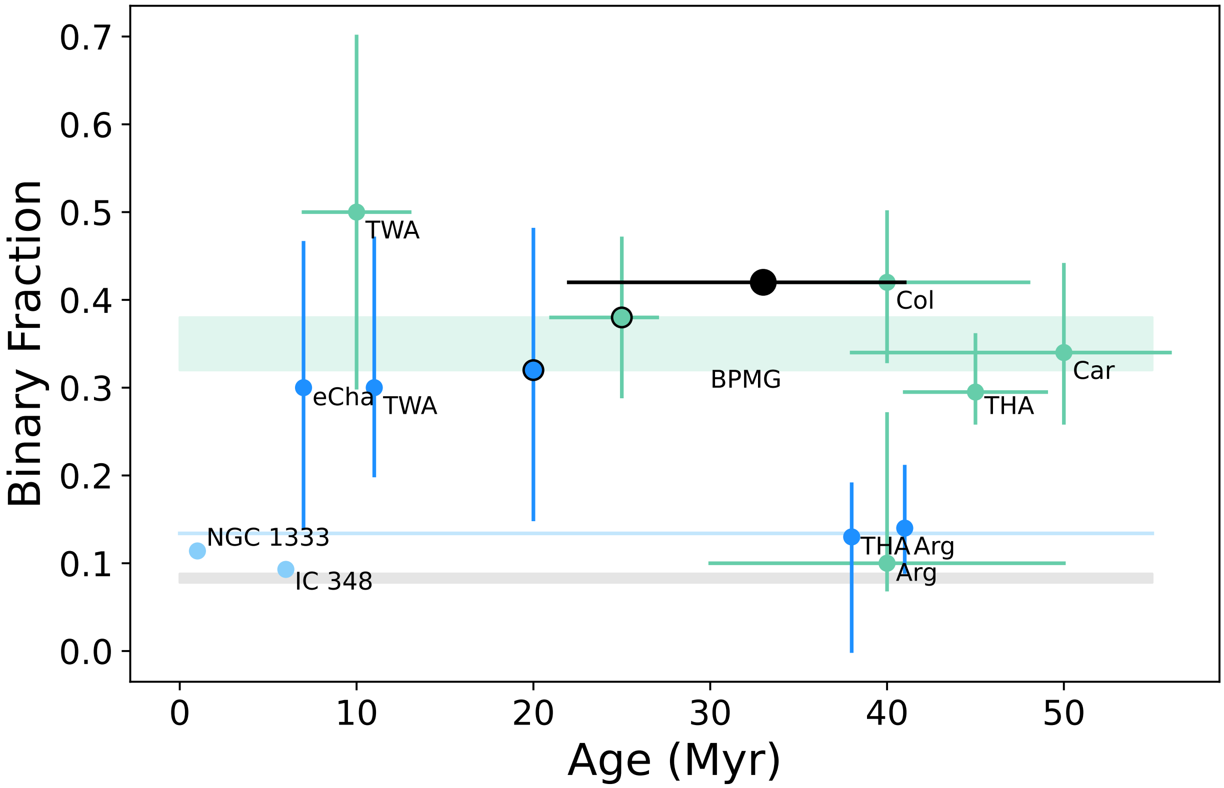

Figure 4.1 Binary fractions from this work compared to those from previous BPMG studies and different YMGs. Estimates for BPMG are outlined in black, and the result from this work is plotted in black. The Kounkel et al. (2019) grey shaded region is an estimate of 8.3±0.5% from RVs and the double-lined spectroscopic binary (SB2) fraction of systems. Jaehnig et al. (2017) give system spectroscopic binary (SB) fractions in star-forming regions (sky blue points), as well as an overall upper limit of 13.4%. Shan et al. (2017) report stellar multiplicity fractions by association (turquoise points) as well as an overall fraction of 35±5% (turquoise shaded region) based on adaptive optics imaging. Zúñiga-Fernández et al. (2021) also report stellar SB fractions for nearby YMGs (dark blue points).

4.2 Age Estimates

We tabulate the age estimates resulting from the isochrone fits in Fig. 4.2 along with the best-fit metric in Table 4.1, and we discuss these results in the following section. We additionally show the LDB fits in Fig. 4.3. For each model we computed the concordance or internal agreement in age results from the three fit methods (*Gaia* CMD, *Gaia*-2MASS CMD, and LDB). This is a χ^2 difference value of the three age results from each model. For the best-fit ages from each of the three fitting methods, we report a 1σ age uncertainty. The age uncertainties were computed by selecting the points on the χ^2 or τ^2 distributions demarcating 68% of the total area under the curve about the minimum χ^2 or τ^2 value.

Table 4.1 BPMG age estimates for each of the 9 evolutionary model sets and 3 age-dating methods. The τ^2 and χ^2 value (minimum) from the best-fit age for a given model and CMD or LBD fit, respectively. The model concordance column is the chi^2 difference between best-fit ages from a given model. The best-fit result from each fit method (*Gaia* CMD, *Gaia*-2MASS CMD, and LDB) is bolded, and the 1σ errors are given in the Age column.

Model	Method	Age (Myr)	$\tau^2_{min,fit}$	$\chi^2_{min,fit}$	Model Concordance (χ^2_{age})
BHAC	G vs. B_P-R_P CMD	12	68.0	–	0.68
BHAC	Ks vs. B_P-R_P CMD	11	62.5	–	
BHAC	LDB	15	–	35.1	
Dartmouth Standard	G vs. B_P-R_P CMD	14	65.1	–	2.80
Dartmouth Standard	**Ks vs. B_P-R_P CMD**	**11^{+4}_{-3}**	**37.8**	–	
Dartmouth Standard	LDB	20	–	27.6	
Dartmouth Magnetic	**G vs. B_P-R_P CMD**	**33^{+9}_{-11}**	**33.2**	–	2.72
Dartmouth Magnetic	Ks vs. B_P-R_P CMD	35	82.9	–	
Dartmouth Magnetic	**LDB**	**23**±8	–	**15.6**	
SPOTS f=0.00	G vs. B_P-R_P CMD	10	210.0	–	10.00
SPOTS f=0.00	Ks vs. B_P-R_P CMD	10	86.7	–	
SPOTS f=0.00	LDB	25	–	26.8	
SPOTS f=0.17	G vs. B_P-R_P CMD	12	140.0	–	2.14
SPOTS f=0.17	Ks vs. B_P-R_P CMD	12	89.8	–	
SPOTS f=0.17	LDB	6.3	–	42.3	
SPOTS f=0.34	G vs. B_P-R_P CMD	20	91.6	–	4.77
SPOTS f=0.34	Ks vs. B_P-R_P CMD	22	76.6	–	
SPOTS f=0.34	LDB	10	–	29.1	
SPOTS f=0.51	G vs. B_P-R_P CMD	32	66.8	–	10.18
SPOTS f=0.51	Ks vs. B_P-R_P CMD	40	43.5	–	
SPOTS f=0.51	LDB	16	–	27.4	
SPOTS f=0.68	G vs. B_P-R_P CMD	45	35.3	–	4.90
SPOTS f=0.68	Ks vs. B_P-R_P CMD	45	38.7	–	
SPOTS f=0.68	LDB	28	–	24.4	
SPOTS f=0.85	G vs. B_P-R_P CMD	50	34.2	–	3.33
SPOTS f=0.85	Ks vs. B_P-R_P CMD	50	44.7	–	
SPOTS f=0.85	LDB	35	–	28.1	

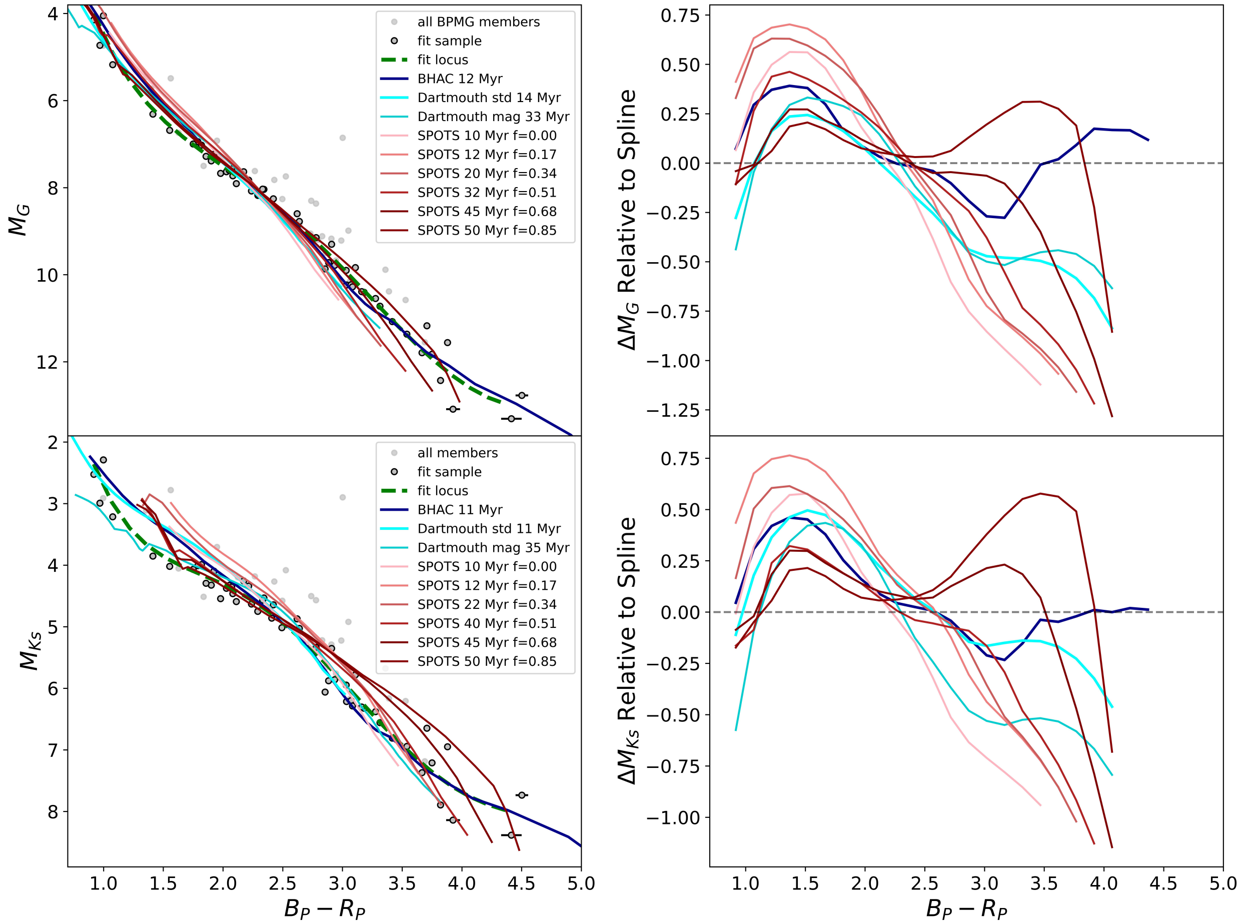

Figure 4.2 *Gaia* (top) and 2MASS-*Gaia* (bottom) color-magnitude diagrams of the single star BPMG sample. All BPMG members confirmed in this study are shown as grey dots, while those passing the binary exclusion and photometric criteria are outlined in black. Only those outlined are used in the isochrone fitting. *Left*: Best-fit isochrones by minimum τ^2. For the SPOTS isochrones, $f\,'$ denotes the revised spot fraction (Eq. 2.1) from YBC corrections. In both panels, we show a best-fit spline to the main BPMG locus in red. *Right*: Each of the nine best-fit isochrone curves subtracted from the BPMG fit locus spline to better visualize the regions of the CMD where the models tend to fit or fail. The τ^2 values for each fit are given in Table 4.1.

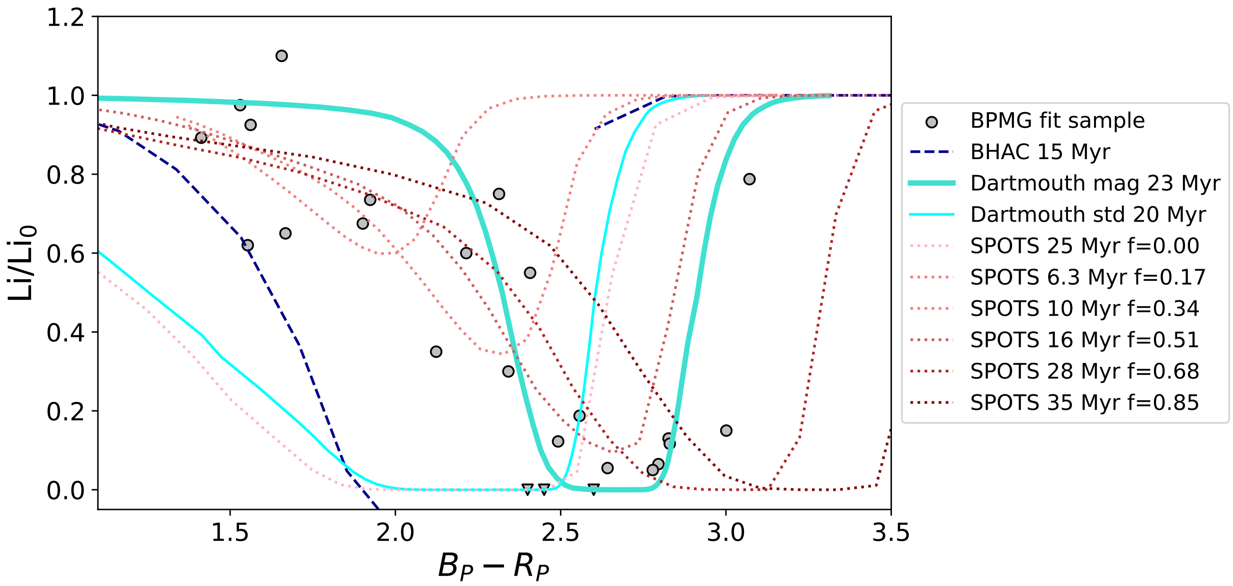

Figure 4.3 Li 6708Å equivalent widths converted to abundances vs. *Gaia* B$_P$-R$_P$ color for BPMG members with Li measurements from the literature. The abundances are computed relative to the primorial ISM value. Points plotted as triangles represent non-detection (upper limits) of lithium. Typical errors are shown in the bottom left. For the incomplete LDB curves from the BHAC models, the fitting sample includes on those within the color ranges covered in the model LDBs. For each model, the best (minumum χ^2) fit model LDB is plotted.

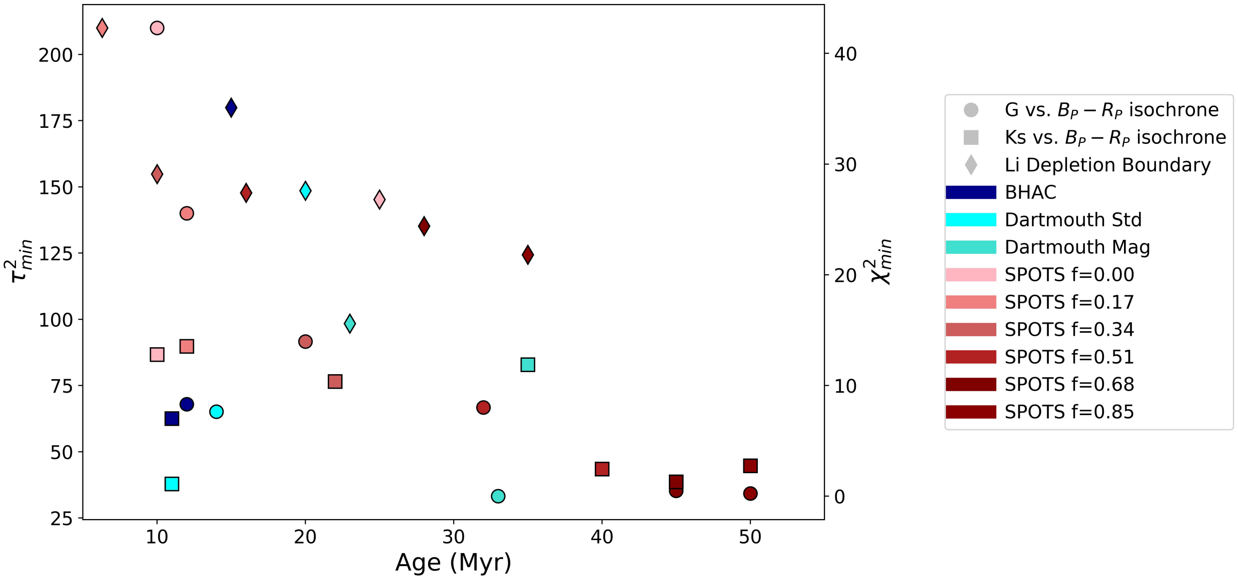

Figure 4.4 The results in Table 4.1 shown graphically. For LDB fits (diamonds), the y-axis is χ^2 scaled on the right, while for CMD fits (circles, squares) the y-axis is τ^2 scaled on the left.

Chapter 5

Discussion

We have presented a detailed sample selection for the Beta Pictoris Moving Group using the most precise available photometry and astrometry and utilizing complete kinematics for membership validation. We further refined this sample by quantitatively identifying older MS interlopers aligned in kinematic space with BPMG, but exhibiting older ages on the color-magnitude diagram. Our catalog contains a total of 106 single and resolved companions, and 47 unresolved binaries. To date, this is the most thorough vetting of binarity in the BPMG sample, and improves upon the previous samples of Gagné & Faherty (2018) and subsequent literature by newly confirming 37 previously identified candidates and rejecting 90 others. The relationship between binary separation, formation, and pre-MS evolution is not well known; this sample of young pre-MS binaries at varying separations paves the way for a detailed study of how the presence of a companion may affect pre-MS spin-down, especially since much of BPMG has been observed by continuous photometric surveys such as TESS.

This sample refinement appears to affect the age estimates quite variably among the different models. Curiously, with the refined and single-star fit sample, one would expect the isochronal ages to bias older (Sullivan & Kraus 2021), but the BHAC and Dartmouth Standard models consistently produce younger ages than the literature employing the same models (e.g., Binks & Jeffries 2014; Malo et al. 2014b). There is notable internal disagreement between the models used in this study, suggesting that the BPMG age determination is largely model-dependent. We show in Fig. 1.1 the results of the present work in comparison to previous literature values. The new age estimates still lie within the uncertainty spread of the literature, but tend to place BPMG at older ages than previously reported. The overall best fits (by minimum τ^2 or χ^2) per method (the two CMDs and LDB) from the 27 estimates are bolded in Table 4.1.

The single best-fit age estimate is supplied by the Dartmouth magnetic models, for producing the lowest τ^2 value in a CMD, and supplying a best-fit model in two of the three fit methods, deeming it the best-performing model overall. The Gaia G vs. B_P-R_P CMD places the BPMG at 33^{+9}_{-11} Myr according to the *Gaia* CMD, while the best-fit LDB suggests 23±8 Myr. Qualitatively, it is clear that the Dartmouth magnetic model is the only appropriate model for LDB fitting; the other models either do not span the color range employed here and/or fail to produce the shape of the BPMG lithium gap at B_P-R_P of $\sim$2.5-3 entirely. The overall best-fit *Gaia*-2MASS isochrone was from the Dartmouth standard model and suggests a much younger age of 11 Myr, but the magnetic model returns a slightly lower τ^2 value. These two isochrone curves (Dartmouth magnetic 33 Myr and standard 11 Myr) are nearly identical, highlighted by the similarity in their offsets from the BPMG locus in the upper right panel of Fig. 4.2 (teal and cyan curves). The magnetic model should be more appropriate, as it should better approximate the actual physics ongoing in these highly active stars (Morris 2020).

One caveat of the isochronal model fitting is that not all models will be appropriate for all stars. We fit the isochrone models for BPMG members spanning a large mass range for homogeneity, however, it is expected that different models are better suited for age determination in different mass ranges. While the lower mass members should be better described by the magnetic and spot fraction models, the higher mass and hotter stars are expected to have fewer spots (Morris 2020). Furthermore, the presence of starspots also affects the structures of stars in different mass ranges. For low-mass, pre-MS stars, starspots slow contraction and spin-down along the Hayashi tracks, leading to inflated radii, from 10% in K-stars up to 40% in M-stars (Jackson & Jeffries 2014).

In the *Gaia* G vs. B_P-R_P CMD, the standard models (BHAC and Dartmouth standard) produce the shape of the BPMG locus well, but slightly overestimate the luminosity of the faintest objects. The standard models do not reproduce the shape of the LDB observed in BPMG. This, in conjunction with the poorer isochrone fits, suggests that the magnetic and spot fraction models are better suited for age-dating BPMG and similar YMGs and young associations. The 2MASS K_s vs. B_P-R_P CMD generally produced poorer isochrone fits across the 9 models. And in both CMDs, the models tend to overestimate the luminosity of the bluest stars.

With increasing spot fraction, the SPOTS models tend to better fit the hottest stars while underestimating the luminosity or color of the coolest members. As mentioned in Sec.3.1, the SPOTS models are not well calibrated in this region of the CMD (Somers et al. 2020). It is possible that the YBC-interpolated isochrones used here are neglecting to account for local extinction around these young stars, where disk materials may still be present or evaporating. Another possibility is that the revised luminosity spot fractions (as opposed to the surface spot fraction) overestimate the true spot fractions of the low mass members, but not the higher mass members. However, lower mass stars are likely to be more active, as they are more rapidly rotating at this stage of the group's evolution. The different SPOTS models, especially the highest spot fraction models ($f' = 0.837$, 0.931) produce the best internal agreement among the three fits. Among the SPOTS models, the overall best-performing is the $f' = 0.837$ model, which suggests and age range of 28-45 Myr. This reinforces the revised age estimated adopted in this study; the better-fitting models push the age estimate older.

The implications of an older age for BPMG on our understanding of disk and planet evolution are several. If the BPMG is indeed older than previously accepted, this contradicts the expected typical disk lifetimes of a few to tens of Myr (Richert et al. 2018). These long-lived disks, now suggested to be even older, have not been well explained, though binary perturbations may play a role. Additionally, any substellar and planetary companions of BPMG members, such as the well-studied systems mentioned in Sec. 1.1, would be more massive than previously determined based on the older age (Sullivan & Kraus 2021).

The revised age estimate presented here is largely dependent upon the models, the methods used to interpolate the isochrones, and the photometric precision of *Gaia* and 2MASS. It is unlikely that *Gaia* is the main source of internal disagreement; it is a homogenous and highly precise dataset. Though, it is certainly possible that the census and binary screen are incomplete. Instead, it appears that the models, while they are appropriate for fitting in some cases, are not quite tuned to the observations compiled in this work. Further spectroscopic follow-up of BPMG members may reveal additional hidden binaries, and deeper searches in to the kinematics may refine the sample further.

Chapter 6

Conclusion

In this study we presented an updated membership census and binary catalog for the Beta Pictoris Moving Group, the nearest and youngest co-moving stellar group in the solar neighborhood. We utilized the latest and most precise space-based astrometry, photometry, and radial velocity data from *Gaia* DR3 to compute precise membership probabilities and identify binaries contaminating the samples of previous photometric age-dating studies. The *Gaia* data was supplemented with ground-based RVs from surveys and literature, and photometry from the 2MASS survey.

With the *Gaia* and RV survey data, we were able to confirm 37 new members of BPMG and reject 90 candidates previously identified in the literature which lacked full kinematic data. We found a multiplicity fraction of 42% using a variety of methods to identify resolved and unresolved binaries among the confirmed BPMG members. The single-star and resolved companion sample was used in age-dating analyses to mitigate the expected age-biasing effects of unidentified binaries in a stellar sample. The multiplicity fraction reported here is in agreement with the literature (e.g., Shan et al. 2017; Zúñiga-Fernández et al. 2021) within errors (Fig. 4.1), following the trend of decreasing binary fraction as a funcin of age (Zúñiga-Fernández et al. 2021). The slightly higher fraction reflects an improved completeness of the binary search, as the previous papers tended to utilize a subset of the binary identification methods from this work (i.e., RVs, AO imaging). The binary fractions from Kounkel et al. (2019) and Jaehnig et al. (2017) in Fig. 4.1 are the ratio of confirmed spectroscopic binaries (SBs) to the total of their sample. Zúñiga-Fernández et al. (2021) also report SB fractions, but extrapolate to an expected occurrence rate. Since we have not investigated SBs in our binary search, our multiplicity fraction represents a lower limit.

We used 9 suites of evolutionary models: the BHAC standard models, Dartmouth standard and magnetic models, and the SPOTS models at 6 discrete spot fractions. We found that the refined sample does not pose as large an effect on the age estimate as the models themselves. From isochrone fitting in two CMDs and from LDB fitting, we find the best-fit age for the BPMG to be 33 Myr. This result is expected from the effect of binaries on stellar luminosities, though the effect is not large. However, the same standard models employed in previous works returned much younger ages of 10-12 Myr, which contradicts the expectation that accounting for binarity would push isochrone ages older.

This study shows that isochrone fitting for young stellar populations is largely sensitive to the models themselves, but that overall, the surface spot and magnetic models out-perform the previous standards.

References

Alonso-Floriano, F. J., Caballero, J. A., Cortés-Contreras, M., Solano, E., & Montes, D. 2015, A&A, 583, A85

Angus, R., Morton, T. D., Foreman-Mackey, D., van Saders, J., Curtis, J., Kane, S. R., Bedell, M., Kiman, R., Hogg, D. W., & Brewer, J. 2019, The Astronomical Journal, 158, 173

Asplund, M., Grevesse, N., Sauval, A. J., & Scott, P. 2009, ARA&A, 47, 481

Baraffe, I., Chabrier, G., Allard, F., & Hauschildt, P. H. 1998, A&A, 337, 403

Baraffe, I., Homeier, D., Allard, F., & Chabrier, G. 2015, A&A, 577, A42

Baraffe, I., Pratt, J., Goffrey, T., Constantino, T., Folini, D., Popov, M. V., Walder, R., & Viallet, M. 2017, ApJ, 845, L6

Bell, C. P. M., Mamajek, E. E., & Naylor, T. 2015, MNRAS, 454, 593

Belokurov, V., Penoyre, Z., Oh, S., Iorio, G., Hodgkin, S., Evans, N. W., Everall, A., Koposov, S. E., Tout, C. A., Izzard, R., Clarke, C. J., & Brown, A. G. A. 2020, MNRAS, 496, 1922

Bildsten, L., Brown, E. F., Matzner, C. D., & Ushomirsky, G. 1997, The Astrophysical Journal, 482, 442

Binks, A. S. & Jeffries, R. D. 2014, MNRAS, 438, L11

—. 2016, MNRAS, 455, 3345

—. 2017, MNRAS, 469, 579

Bowler, B. P., Hinkley, S., Ziegler, C., Baranec, C., Gizis, J. E., Law, N. M., Liu, M. C., Shah, V. S., Shkolnik, E. L., Riaz, B., & Riddle, R. 2019, ApJ, 877, 60

Burke, C. J., Pinsonneault, M. H., & Sills, A. 2004, The Astrophysical Journal, 604, 272

Cale, B. L., Reefe, M., Plavchan, P., Tanner, A., Gaidos, E., Gagne, J., Gao, P., Kane, S. R., Bejar, V. J. S., Lodieu, N., Anglada-Escude, G., Ribas, I., Palle, E., Quirrenbach, A., Amado, P. J., Reiners, A., Caballero, J. A., Rosa Zapatero Osorio, M., Dreizler, S., Howard, A. W., Fulton, B. J., Xuesong Wang, S., Collins, K. I., El Mufti, M., Wittrock, J., Gilbert, E. A., Barclay, T., Klein, B., Martioli, E., Wittenmyer, R., Wright, D., Addison, B., Hirano, T., Tamura, M., Kotani, T., Narita, N., Vermilion, D., Lee, R. A., Geneser, C., Teske, J., Quinn, S. N., Latham, D. W., Esquerdo, G. A., Calkins, M. L., Berlind, P., Zohrabi, F., Stibbards, C., Kotnana, S., Jenkins, J., Twicken, J. D., Henze, C., Kidwell, R., Burke, C., Villasenor, J., & Boyd, P. 2021, AJ, 162, 295

Chabrier, G. & Baraffe, I. 1997, A&A, 327, 1039

Chance, Q., Foreman-Mackey, D., Ballard, S., Casey, A., David, T., & Price-Whelan, A. 2022, arXiv e-prints, arXiv:2206.11275

Chen, Y., Girardi, L., Fu, X., Bressan, A., Aringer, B., Dal Tio, P., Pastorelli, G., Marigo, P., Costa, G., & Zhang, X. 2019, A&A, 632, A105

Crundall, T. D., Ireland, M. J., Krumholz, M. R., Federrath, C., Žerjal, M., & Hansen, J. T. 2019, MNRAS, 489, 3625

Dotter, A. 2016, ApJS, 222, 8

Dotter, A., Chaboyer, B., Jevremović, D., Kostov, V., Baron, E., & Ferguson, J. W. 2008, ApJS, 178, 89

Duchêne, G. & Kraus, A. 2013, Annual Review of Astronomy and Astrophysics, 51, 269

Evans, D. W., Riello, M., De Angeli, F., Carrasco, J. M., Montegriffo, P., Fabricius, C., Jordi, C., Palaversa, L., Diener, C., Busso, G., Cacciari, C., van Leeuwen, F., Burgess, P. W., Davidson, M., Harrison, D. L., Hodgkin, S. T., Pancino, E., Richards, P. J., Altavilla, G., Balaguer-Núñez, L., Barstow, M. A., Bellazzini, M., Brown, A. G. A., Castellani, M., Cocozza, G., De Luise, F., Delgado, A., Ducourant, C., Galleti, S., Gilmore, G., Giuffrida, G., Holl, B., Kewley, A., Koposov, S. E., Marinoni, S., Marrese, P. M., Osborne, P. J., Piersimoni, A., Portell, J., Pulone, L., Ragaini, S., Sanna, N., Terrett, D., Walton, N. A., Wevers, T., & Wyrzykowski, Ł. 2018, A&A, 616, A4

Faherty, J. K., Bochanski, J. J., Gagné, J., Nelson, O., Coker, K., Smithka, I., Desir, D., & Vasquez, C. 2018, ApJ, 863, 91

Feiden, G. A. 2016, A&A, 593, A99

Feiden, G. A. & Chaboyer, B. 2012, ApJ, 761, 30

Feiden, G. A., Jones, J., & Chaboyer, B. 2015, in Cambridge Workshop on Cool Stars, Stellar Systems, and the Sun, Vol. 18, 18th Cambridge Workshop on Cool Stars, Stellar Systems, and the Sun, 171–176

Fitton, S., Tofflemire, B. M., & Kraus, A. L. 2022, Research Notes of the AAS, 6, 18

Gagné, J. & Faherty, J. K. 2018, ApJ, 862, 138

Gagné, J., Mamajek, E. E., Malo, L., Riedel, A., Rodriguez, D., Lafrenière, D., Faherty, J. K., Roy-Loubier, O., Pueyo, L., Robin, A. C., & Doyon, R. 2018, ApJ, 856, 23

Gaia Collaboration, Brown, A. G. A., Vallenari, A., Prusti, T., de Bruijne, J. H. J., Babusiaux, C., Biermann, M., Creevey, O. L., Evans, D. W., Eyer, L., Hutton, A., Jansen, F., Jordi, C., Klioner, S. A., Lammers, U., Lindegren, L., Luri, X., Mignard, F., Panem, C., Pourbaix, D., Randich, S., Sartoretti, P., Soubiran, C., Walton, N. A., Arenou, F., Bailer-Jones, C. A. L., Bastian, U., Cropper, M., Drimmel, R., Katz, D., Lattanzi, M. G., van Leeuwen, F., Bakker, J., Cacciari, C., Castañeda, J., De Angeli, F., Ducourant, C., Fabricius, C., Fouesneau, M., Frémat, Y., Guerra, R., Guerrier, A., Guiraud, J., Jean-Antoine Piccolo, A., Masana, E., Messineo, R., Mowlavi, N., Nicolas, C., Nienartowicz, K., Pailler, F., Panuzzo, P., Riclet, F., Roux, W., Seabroke, G. M., Sordo, R., Tanga, P., Thévenin, F., Gracia-Abril, G., Portell, J., Teyssier, D., Altmann, M., Andrae, R., Bellas-Velidis, I., Benson, K., Berthier, J., Blomme, R., Brugaletta, E., Burgess,

P. W., Busso, G., Carry, B., Cellino, A., Cheek, N., Clementini, G., Damerdji, Y., Davidson, M., Delchambre, L., Dell'Oro, A., Fernández-Hernández, J., Galluccio, L., García-Lario, P., Garcia-Reinaldos, M., González-Núñez, J., Gosset, E., Haigron, R., Halbwachs, J. L., Hambly, N. C., Harrison, D. L., Hatzidimitriou, D., Heiter, U., Hernández, J., Hestroffer, D., Hodgkin, S. T., Holl, B., Janßen, K., Jevardat de Fombelle, G., Jordan, S., Krone-Martins, A., Lanzafame, A. C., Löffler, W., Lorca, A., Manteiga, M., Marchal, O., Marrese, P. M., Moitinho, A., Mora, A., Muinonen, K., Osborne, P., Pancino, E., Pauwels, T., Petit, J. M., Recio-Blanco, A., Richards, P. J., Riello, M., Rimoldini, L., Robin, A. C., Roegiers, T., Rybizki, J., Sarro, L. M., Siopis, C., Smith, M., Sozzetti, A., Ulla, A., Utrilla, E., van Leeuwen, M., van Reeven, W., Abbas, U., Abreu Aramburu, A., Accart, S., Aerts, C., Aguado, J. J., Ajaj, M., Altavilla, G., Álvarez, M. A., Álvarez Cid-Fuentes, J., Alves, J., Anderson, R. I., Anglada Varela, E., Antoja, T., Audard, M., Baines, D., Baker, S. G., Balaguer-Núñez, L., Balbinot, E., Balog, Z., Barache, C., Barbato, D., Barros, M., Barstow, M. A., Bartolomé, S., Bassilana, J. L., Bauchet, N., Baudesson-Stella, A., Becciani, U., Bellazzini, M., Bernet, M., Bertone, S., Bianchi, L., Blanco-Cuaresma, S., Boch, T., Bombrun, A., Bossini, D., Bouquillon, S., Bragaglia, A., Bramante, L., Breedt, E., Bressan, A., Brouillet, N., Bucciarelli, B., Burlacu, A., Busonero, D., Butkevich, A. G., Buzzi, R., Caffau, E., Cancelliere, R., Cánovas, H., Cantat-Gaudin, T., Carballo, R., Carlucci, T., Carnerero, M. I., Carrasco, J. M., Casamiquela, L., Castellani, M., Castro-Ginard, A., Castro Sampol, P., Chaoul, L., Charlot, P., Chemin, L., Chiavassa, A., Cioni, M. R. L., Comoretto, G., Cooper, W. J., Cornez, T., Cowell, S., Crifo, F., Crosta, M., Crowley, C., Dafonte, C., Dapergolas, A., David, M., David, P., de Laverny, P., De Luise, F., De March, R., De Ridder, J., de Souza, R., de Teodoro, P., de Torres, A., del Peloso, E. F., del Pozo, E., Delbo, M., Delgado, A., Delgado, H. E., Delisle, J. B., Di Matteo, P., Diakite, S., Diener, C., Distefano, E., Dolding, C., Eappachen, D., Edvardsson, B., Enke, H., Esquej, P., Fabre, C., Fabrizio, M., Faigler, S., Fedorets, G., Fernique, P., Fienga, A., Figueras, F., Fouron, C., Fragkoudi, F., Fraile, E., Franke, F., Gai, M., Garabato, D., Garcia-Gutierrez, A., García-Torres, M., Garofalo, A., Gavras, P., Gerlach, E., Geyer, R., Giacobbe, P., Gilmore, G., Girona, S., Giuffrida, G., Gomel, R., Gomez, A., Gonzalez-Santamaria, I., González-Vidal, J. J., Granvik, M., Gutiérrez-Sánchez, R., Guy, L. P., Hauser, M., Haywood, M., Helmi, A., Hidalgo, S. L., Hilger, T., Hładczuk, N., Hobbs, D., Holland, G., Huckle, H. E., Jasniewicz, G., Jonker, P. G., Juaristi Campillo, J., Julbe, F., Karbevska, L., Kervella, P., Khanna, S., Kochoska, A., Kontizas, M., Kordopatis, G., Korn, A. J., Kostrzewa-Rutkowska, Z., Kruszyńska, K., Lambert, S., Lanza, A. F., Lasne, Y., Le Campion, J. F., Le Fustec, Y., Lebreton, Y., Lebzelter, T., Leccia, S., Leclerc, N., Lecoeur-Taibi, I., Liao, S., Licata, E., Lindstrøm, E. P., Lister, T. A., Livanou, E., Lobel, A., Madrero Pardo, P., Managau, S., Mann, R. G., Marchant, J. M., Marconi, M., Marcos Santos, M. M. S., Marinoni, S., Marocco, F., Marshall, D. J., Martin Polo, L., Martín-Fleitas, J. M., Masip, A., Massari, D., Mastrobuono-Battisti, A., Mazeh, T., McMillan, P. J., Messina, S., Michalik, D., Millar, N. R., Mints, A., Molina, D., Molinaro, R., Molnár, L., Montegriffo, P., Mor, R., Morbidelli, R., Morel, T., Morris, D., Mulone, A. F., Munoz, D., Muraveva, T., Murphy, C. P., Musella, I., Noval, L., Ordénovic, C., Orrù, G., Osinde, J., Pagani, C., Pagano, I., Palaversa, L., Palicio, P. A., Panahi, A., Pawlak, M., Peñalosa Esteller, X., Penttilä, A., Piersimoni, A. M., Pineau, F. X., Plachy, E., Plum, G., Poggio, E., Poretti, E., Poujoulet, E., Prša, A., Pulone, L., Racero, E., Ragaini, S., Rainer, M., Raiteri, C. M., Rambaux, N., Ramos, P., Ramos-Lerate, M., Re Fiorentin, P., Regibo, S., Reylé, C., Ripepi, V., Riva, A., Rixon, G., Robichon, N., Robin, C., Roelens, M., Rohrbasser, L., Romero-Gómez, M., Rowell, N., Royer, F., Rybicki, K. A., Sadowski, G., Sagristà Sellés, A., Sahlmann, J., Salgado, J., Salguero, E., Samaras, N., Sanchez Gimenez, V., Sanna, N., Santoveña, R., Sarasso, M., Schultheis, M., Sciacca, E., Segol, M., Segovia, J. C., Ségransan, D., Semeux, D., Shahaf, S., Siddiqui, H. I., Siebert, A., Siltala, L., Slezak, E., Smart, R. L., Solano, E., Solitro, F., Souami, D., Souchay, J., Spagna, A., Spoto, F., Steele, I. A., Steidelmüller, H., Stephenson, C. A., Süveges, M., Szabados, L., Szegedi-Elek, E., Taris, F., Tauran, G., Taylor, M. B., Teixeira, R., Thuillot, W., Tonello, N., Torra, F., Torra, J., Turon, C., Unger, N., Vaillant, M., van Dillen, E., Vanel, O., Vecchiato, A., Viala, Y., Vicente, D., Voutsinas, S., Weiler, M., Wevers, T., Wyrzykowski, Ł., Yoldas, A., Yvard, P., Zhao, H., Zorec, J., Zucker, S., Zurbach, C., & Zwitter, T. 2021, A&A, 649, A1

Gaia Collaboration, Prusti, T., de Bruijne, J. H. J., Brown, A. G. A., Vallenari, A., Babusiaux, C., Bailer-Jones, C. A. L., Bastian, U., Biermann, M., Evans, D. W., Eyer, L., Jansen, F., Jordi, C., Klioner, S. A., Lammers, U., Lindegren, L., Luri, X., Mignard, F., Milligan, D. J., Panem, C., Poinsignon, V., Pourbaix, D., Randich, S., Sarri, G., Sartoretti, P., Siddiqui, H. I., Soubiran, C., Valette, V., van Leeuwen, F., Walton, N. A., Aerts, C., Arenou, F., Cropper, M., Drimmel, R., Høg, E., Katz, D., Lattanzi, M. G., O'Mullane, W., Grebel, E. K., Holland, A. D., Huc, C., Passot, X., Bramante, L., Cacciari, C., Castañeda, J., Chaoul, L., Cheek, N., De Angeli, F., Fabricius, C., Guerra, R., Hernández, J., Jean-Antoine-Piccolo, A., Masana, E., Messineo, R., Mowlavi, N., Nienartowicz, K., Ordóñez-Blanco, D., Panuzzo, P., Portell, J., Richards, P. J., Riello, M., Seabroke, G. M., Tanga, P., Thévenin, F., Torra, J., Els, S. G., Gracia-Abril, G., Comoretto, G., Garcia-Reinaldos, M., Lock, T., Mercier, E., Altmann, M., Andrae, R., Astraatmadja, T. L., Bellas-Velidis, I., Benson, K., Berthier, J., Blomme, R., Busso, G., Carry, B., Cellino, A., Clementini, G., Cowell, S., Creevey, O., Cuypers, J., Davidson, M., De Ridder, J., de Torres, A., Delchambre, L., Dell'Oro, A., Ducourant, C., Frémat, Y., García-Torres, M., Gosset, E., Halbwachs, J. L., Hambly, N. C., Harrison, D. L., Hauser, M., Hestroffer, D., Hodgkin, S. T., Huckle, H. E., Hutton, A., Jasniewicz, G., Jordan, S., Kontizas, M., Korn, A. J., Lanzafame, A. C., Manteiga, M., Moitinho, A., Muinonen, K., Osinde, J., Pancino, E., Pauwels, T., Petit, J. M., Recio-Blanco, A., Robin, A. C., Sarro, L. M., Siopis, C., Smith, M., Smith, K. W., Sozzetti, A., Thuillot, W., van Reeven, W., Viala, Y., Abbas, U., Abreu Aramburu, A., Accart, S., Aguado, J. J., Allan, P. M., Allasia, W., Altavilla, G., Álvarez, M. A., Alves, J., Anderson, R. I., Andrei, A. H., Anglada Varela, E., Antiche, E., Antoja, T., Antón, S., Arcay, B., Atzei, A., Ayache, L., Bach, N., Baker, S. G., Balaguer-Núñez, L., Barache, C., Barata, C., Barbier, A., Barblan, F., Baroni, M., Barrado y Navascués, D., Barros, M., Barstow, M. A., Becciani, U., Bellazzini, M., Bellei, G., Bello García, A., Belokurov, V., Bendjoya, P., Berihuete, A., Bianchi, L., Bienaymé, O., Billebaud, F., Blagorodnova, N., Blanco-Cuaresma, S., Boch, T., Bombrun, A., Borrachero, R., Bouquillon, S., Bourda, G., Bouy, H., Bragaglia, A., Breddels, M. A., Brouillet, N., Brüsemeister, T., Bucciarelli, B., Budnik, F., Burgess, P., Burgon, R., Burlacu, A., Busonero, D., Buzzi, R., Caffau, E., Cambras, J., Campbell, H., Cancelliere, R., Cantat-Gaudin, T., Carlucci, T., Carrasco, J. M., Castellani, M., Charlot, P., Charnas, J., Charvet, P., Chassat, F., Chiavassa, A., Clotet, M., Cocozza, G., Collins, R. S., Collins, P., Costigan, G., Crifo, F., Cross, N. J. G., Crosta, M., Crowley, C., Dafonte, C., Damerdji, Y., Dapergolas, A., David, P., David, M., De Cat, P., de Felice, F., de Laverny, P., De Luise, F., De March, R., de Martino, D., de Souza, R., Debosscher, J., del Pozo, E., Delbo, M., Delgado, A., Delgado, H. E., di Marco, F., Di Matteo, P., Diakite, S., Distefano, E., Dolding, C., Dos Anjos, S., Drazinos, P., Durán, J., Dzigan, Y., Ecale, E., Edvardsson, B., Enke, H., Erdmann, M., Escolar, D., Espina, M., Evans, N. W., Eynard Bontemps, G., Fabre, C., Fabrizio, M., Faigler, S., Falcão, A. J., Farràs Casas, M., Faye, F., Federici, L., Fedorets, G., Fernández-Hernández, J., Fernique, P., Fienga, A., Figueras, F., Filippi, F., Findeisen, K., Fonti, A., Fouesneau, M., Fraile, E., Fraser, M., Fuchs, J., Furnell, R., Gai, M., Galleti, S., Galluccio, L., Garabato, D., García-Sedano, F., Garé, P., Garofalo, A., Garralda, N., Gavras, P., Gerssen, J., Geyer, R., Gilmore, G., Girona, S., Giuffrida, G., Gomes, M., González-Marcos, A., González-Núñez, J., González-Vidal, J. J., Granvik, M., Guerrier, A., Guillout, P., Guiraud, J., Gúrpide, A., Gutiérrez-Sánchez, R., Guy, L. P., Haigron, R., Hatzidimitriou, D., Haywood, M., Heiter, U., Helmi, A., Hobbs, D., Hofmann, W., Holl, B., Holland, G., Hunt, J. A. S., Hypki, A., Icardi, V., Irwin, M., Jevardat de Fombelle, G., Jofré, P., Jonker, P. G., Jorissen, A., Julbe, F., Karampelas, A., Kochoska, A., Kohley, R., Kolenberg, K., Kontizas, E., Koposov, S. E., Kordopatis, G., Koubsky, P., Kowalczyk, A., Krone-Martins, A., Kudryashova, M., Kull, I., Bachchan, R. K., Lacoste-Seris, F., Lanza, A. F., Lavigne, J. B., Le Poncin-Lafitte, C., Lebreton, Y., Lebzelter, T., Leccia, S., Leclerc, N., Lecoeur-Taibi, I., Lemaitre, V., Lenhardt, H., Leroux, F., Liao, S., Licata, E., Lindstrøm, H. E. P., Lister, T. A., Livanou, E., Lobel, A., Löffler, W., López, M., Lopez-Lozano, A., Lorenz, D., Loureiro, T., MacDonald, I., Magalhães Fernandes, T., Managau, S., Mann, R. G., Mantelet, G., Marchal, O., Marchant, J. M., Marconi, M., Marie, J., Marinoni, S., Marrese, P. M., Marschalkó, G., Marshall, D. J., Martín-Fleitas, J. M., Martino, M., Mary, N., Matijevič, G., Mazeh, T., McMillan, P. J., Messina, S., Mestre, A., Michalik, D., Millar, N. R., Miranda, B. M. H., Molina, D., Molinaro, R., Molinaro, M., Molnár, L., Moniez, M., Montegriffo, P., Monteiro, D., Mor, R., Mora, A., Morbidelli, R., Morel, T., Morgenthaler, S., Morley, T., Morris, D., Mulone, A. F., Muraveva, T., Musella, I., Narbonne, J., Nelemans, G., Nicastro, L., Noval, L., Ordénovic, C., Ordieres-Meré, J., Osborne, P., Pagani, C., Pagano, I., Pailler, F., Palacin, H., Palaversa, L., Parsons, P., Paulsen, T., Pecoraro, M., Pedrosa, R., Pentikäinen, H., Pereira, J., Pichon, B., Piersimoni, A. M., Pineau, F. X., Plachy, E., Plum, G., Poujoulet, E., Prša, A., Pulone, L., Ragaini, S., Rago, S., Rambaux, N., Ramos-Lerate, M., Ranalli, P., Rauw, G., Read, A., Regibo, S., Renk, F., Reylé, C., Ribeiro, R. A., Rimoldini, L., Ripepi, V., Riva, A., Rixon, G., Roelens, M., Romero-Gómez, M., Rowell, N., Royer, F., Rudolph, A., Ruiz-Dern, L., Sadowski, G., Sagristà Sellés, T., Sahlmann, J., Salgado, J., Salguero, E., Sarasso, M., Savietto, H., Schnorhk, A., Schultheis, M., Sciacca, E., Segol, M., Segovia, J. C., Segransan, D., Serpell, E., Shih, I. C., Smareglia, R., Smart, R. L., Smith, C., Solano, E., Solitro, F., Sordo, R., Soria Nieto, S., Souchay, J., Spagna, A., Spoto, F., Stampa, U., Steele, I. A., Steidelmüller, H., Stephenson, C. A., Stoev, H., Suess, F. F., Süveges, M., Surdej, J., Szabados, L., Szegedi-Elek, E., Tapiador, D., Taris, F., Tauran, G., Taylor, M. B., Teixeira, R., Terrett, D., Tingley, B., Trager, S. C., Turon, C., Ulla, A., Utrilla, E., Valentini, G., van Elteren, A., Van Hemelryck, E., van Leeuwen, M., Varadi, M., Vecchiato, A., Veljanoski, J., Via, T., Vicente, D., Vogt, S., Voss, H., Votruba, V., Voutsinas, S., Walmsley, G., Weiler, M., Weingrill, K., Werner, D., Wevers, T., Whitehead, G., Wyrzykowski, Ł., Yoldas, A., Žerjal, M., Zucker, S., Zurbach, C., Zwitter, T., Alecu, A., Allen, M., Allende Prieto, C., Amorim, A., Anglada-Escudé, G., Arsenijevic, V., Azaz, S., Balm, P., Beck, M., Bernstein, H. H., Bigot, L., Bijaoui, A., Blasco, C., Bonfigli, M., Bono, G., Boudreault, S., Bressan, A., Brown, S., Brunet, P. M., Bunclark, P., Buonanno, R., Butkevich, A. G., Carret, C., Carrion, C., Chemin, L., Chéreau, F., Corcione, L., Darmigny, E., de Boer, K. S., de Teodoro, P., de Zeeuw, P. T., Delle Luche, C., Domingues, C. D., Dubath, P., Fodor, F., Frézouls, B., Fries, A., Fustes, D., Fyfe, D., Gallardo, E., Gallegos, J., Gardiol, D., Gebran, M., Gomboc, A., Gómez, A., Grux, E., Gueguen, A., Heyrovsky, A., Hoar, J., Iannicola, G., Isasi Parache, Y., Janotto, A. M., Joliet, E., Jonckheere, A., Keil, R., Kim, D. W., Klagyivik, P., Klar, J., Knude, J., Kochukhov, O., Kolka, I., Kos, J., Kutka, A., Lainey, V., LeBouquin, D., Liu, C., Loreggia, D., Makarov, V. V., Marseille, M. G., Martayan, C., Martinez-Rubi, O., Massart, B., Meynadier, F., Mignot, S., Munari, U., Nguyen, A. T., Nordlander, T., Ocvirk, P., O'Flaherty, K. S., Olias Sanz, A., Ortiz, P., Osorio, J., Oszkiewicz, D., Ouzounis, A., Palmer, M., Park, P., Pasquato, E., Peltzer, C., Peralta, J., Péturaud, F., Pieniluoma, T., Pigozzi, E., Poels, J., Prat, G., Prod'homme, T., Raison, F., Rebordao, J. M., Risquez, D., Rocca-Volmerange, B., Rosen, S., Ruiz-Fuertes, M. I., Russo, F., Sembay, S., Serraller Vizcaino, I., Short, A., Siebert, A., Silva, H., Sinachopoulos, D., Slezak, E., Soffel, M., Sosnowska, D., Straižys, V., ter Linden, M., Terrell, D., Theil, S., Tiede, C., Troisi, L., Tsalmantza, P., Tur, D., Vaccari, M., Vachier, F., Valles, P., Van Hamme, W., Veltz, L., Virtanen, J., Wallut, J. M., Wichmann, R., Wilkinson, M. I., Ziaeepour, H., & Zschocke, S. 2016, A&A, 595, A1

Ghez, A. M., McCarthy, D. W., Patience, J. L., & Beck, T. L. 1997, ApJ, 481, 378

Green, G. 2018, The Journal of Open Source Software, 3, 695

Grevesse, N., Asplund, M., & Sauval, A. J. 2007, Space Sci. Rev., 130, 105

Guiglion, G., Matijevič, G., Queiroz, A. B. A., Valentini, M., Steinmetz, M., Chiappini, C., Grebel, E. K., McMillan, P. J., Kordopatis, G., Kunder, A., Zwitter, T., Khalatyan, A., Anders, F., Enke, H., Minchev, I., Monari, G., Wyse, R. F. G., Bienaymé, O., Bland-Hawthorn, J., Gibson, B. K., Navarro, J. F., Parker, Q., Reid, W., Seabroke, G. M., & Siebert, A. 2020, A&A, 644, A168

Gustafsson, B., Edvardsson, B., Eriksson, K., Jørgensen, U. G., Nordlund, Å., & Plez, B. 2008, A&A, 486, 951

Haemmerlé, L., Eggenberger, P., Ekström, S., Georgy, C., Meynet, G., Postel, A., Audard, M., Sørensen, M., & Fragos, T. 2019, A&A, 624, A137

Haemmerlé, L., Eggenberger, P., Meynet, G., Maeder, A., Charbonnel, C., & Klessen, R. S. 2017, A&A, 602, A17

Hauschildt, P. H., Allard, F., & Baron, E. 1999, ApJ, 512, 377

Hodapp, K. W., Jensen, J. B., Irwin, E. M., Yamada, H., Chung, R., Fletcher, K., Robertson, L., Hora, J. L., Simons, D. A., Mays, W., Nolan, R., Bec, M., Merrill, M., & Fowler, A. M. 2003, PASP, 115, 1388

Jackson, R. J. & Jeffries, R. D. 2014, Monthly Notices of the Royal Astronomical Society, 441, 2111

Jaehnig, K., Bird, J. C., Stassun, K. G., Da Rio, N., Tan, J. C., Cotaar, M., & Somers, G. 2017, ApJ, 851, 14

Kalas, P., Liu, M. C., & Matthews, B. C. 2004, Science, 303, 1990

Kippenhahn, R., Weigert, A., & Weiss, A. 2013, Stellar Structure and Evolution

Kiss, L. L., Moór, A., Szalai, T., Kovács, J., Bayliss, D., Gilmore, G. F., Bienaymé, O., Binney, J., Bland-Hawthorn, J., Campbell, R., Freeman, K. C., Fulbright, J. P., Gibson, B. K., Grebel, E. K., Helmi, A., Munari, U., Navarro, J. F., Parker, Q. A., Reid, W., Seabroke, G. M., Siebert, A., Siviero, A., Steinmetz, M., Watson, F. G., Williams, M., Wyse, R. F. G., & Zwitter, T. 2011, MNRAS, 411, 117

Kounkel, M., Covey, K., Moe, M., Kratter, K. M., Suárez, G., Stassun, K. G., Román-Zúñiga, C., Hernandez, J., Kim, J. S., Peña Ramírez, K., Roman-Lopes, A., Stringfellow, G. S., Jaehnig, K. O., Borissova, J., Tofflemire, B., Krolikowski, D., Rizzuto, A., Kraus, A., Badenes, C., Longa-Peña, P., Gómez Maqueo Chew, Y., Barba, R., Nidever, D. L., Brown, C., De Lee, N., Pan, K., Bizyaev, D., Oravetz, D., & Oravetz, A. 2019, AJ, 157, 196

Krumholz, M. R., McKee, C. F., & Bland-Hawthorn, J. 2019, ARA&A, 57, 227

Kunitomo, M., Guillot, T., Takeuchi, T., & Ida, S. 2017, A&A, 599, A49

Lagrange, A. M., Bonnefoy, M., Chauvin, G., Apai, D., Ehrenreich, D., Boccaletti, A., Gratadour, D., Rouan, D., Mouillet, D., Lacour, S., & Kasper, M. 2010, Science, 329, 57

Lagrange, A. M., Rubini, P., Nowak, M., Lacour, S., Grandjean, A., Boccaletti, A., Langlois, M., Delorme, P., Gratton, R., Wang, J., Flasseur, O., Galicher, R., Kral, Q., Meunier, N., Beust, H., Babusiaux, C., Le Coroller, H., Thebault, P., Kervella, P., Zurlo, A., Maire, A. L., Wahhaj, Z., Amorim, A., Asensio-Torres, R., Benisty, M., Berger, J. P., Bonnefoy, M., Brandner, W., Cantalloube, F., Charnay, B., Chauvin, G., Choquet, E., Clénet, Y., Christiaens, V., Coudé Du Foresto, V., de Zeeuw, P. T., Desidera, S., Duvert, G., Eckart, A., Eisenhauer, F., Galland, F., Gao, F., Garcia, P., Garcia Lopez, R., Gendron, E., Genzel, R., Gillessen, S., Girard, J., Hagelberg, J., Haubois, X., Henning, T., Heissel, G., Hippler, S., Horrobin, M., Janson, M., Kammerer, J., Kenworthy, M., Keppler, M., Kreidberg, L., Lapeyrère, V., Le Bouquin, J. B., Léna, P., Mérand, A., Messina, S., Mollière, P., Monnier, J. D., Ott, T., Otten, G., Paumard, T., Paladini, C., Perraut, K., Perrin, G., Pueyo, L., Pfuhl, O., Rodet, L., Rodriguez-Coira, G., Rousset, G., Samland, M., Shangguan, J., Schmidt, T., Straub, O., Straubmeier, C., Stolker, T., Vigan, A., Vincent, F., Widmann, F., Woillez, J., & Gravity Collaboration. 2020, A&A, 642, A18

Lecavelier Des Etangs, A., Perrin, G., Ferlet, R., Vidal Madjar, A., Colas, F., Buil, C., Sevre, F., Arlot, J. E., Beust, H., Lagrange Henri, A. M., Lecacheux, J., Deleuil, M., & Gry, C. 1993, A&A, 274, 877

Lee, J. & Song, I. 2018, MNRAS, 475, 2955

Leike, R. H., Glatzle, M., & Enßlin, T. A. 2020, A&A, 639, A138

Lenzen, R., Hartung, M., Brandner, W., Finger, G., Hubin, N. N., Lacombe, F., Lagrange, A.-M., Lehnert, M. D., Moorwood, A. F. M., & Mouillet, D. 2003, in Society of Photo-Optical Instrumentation Engineers (SPIE) Conference Series, Vol. 4841, Instrument Design and Performance for Optical/Infrared Ground-based Telescopes, ed. M. Iye & A. F. M. Moorwood, 944–952

Liu, M. C., Magnier, E. A., Deacon, N. R., Allers, K. N., Dupuy, T. J., Kotson, M. C., Aller, K. M., Burgett, W. S., Chambers, K. C., Draper, P. W., Hodapp, K. W., Jedicke, R., Kaiser, N., Kudritzki, R. P., Metcalfe, N., Morgan, J. S., Price, P. A., Tonry, J. L., & Wainscoat, R. J. 2013, ApJ, 777, L20

Macintosh, B., Graham, J. R., Barman, T., De Rosa, R. J., Konopacky, Q., Marley, M. S., Marois, C., Nielsen, E. L., Pueyo, L., Rajan, A., Rameau, J., Saumon, D., Wang, J. J., Patience, J., Ammons, M., Arriaga, P., Artigau, E., Beckwith, S., Brewster, J., Bruzzone, S., Bulger, J., Burningham, B., Burrows, A. S., Chen, C., Chiang, E., Chilcote, J. K., Dawson, R. I., Dong, R., Doyon, R., Draper, Z. H., Duchêne, G., Esposito, T. M., Fabrycky, D., Fitzgerald, M. P., Follette, K. B., Fortney, J. J., Gerard, B., Goodsell, S., Greenbaum, A. Z., Hibon, P., Hinkley, S., Cotten, T. H., Hung, L. W., Ingraham, P., Johnson-Groh, M., Kalas, P., Lafreniere, D., Larkin, J. E., Lee, J., Line, M., Long, D., Maire, J., Marchis, F., Matthews, B. C., Max, C. E., Metchev, S., Millar-Blanchaer, M. A., Mittal, T., Morley, C. V., Morzinski, K. M., Murray-Clay, R., Oppenheimer, R., Palmer, D. W., Patel, R., Perrin, M. D., Poyneer, L. A., Rafikov, R. R., Rantakyrö, F. T., Rice, E. L., Rojo, P., Rudy, A. R., Ruffio, J. B., Ruiz, M. T., Sadakuni, N., Saddlemyer, L., Salama, M., Savransky, D., Schneider, A. C., Sivaramakrishnan, A., Song, I., Soummer, R., Thomas, S., Vasisht, G., Wallace, J. K., Ward-Duong, K., Wiktorowicz, S. J., Wolff, S. G., & Zuckerman, B. 2015, Science, 350, 64

Malo, L., Artigau, É., Doyon, R., Lafrenière, D., Albert, L., & Gagné, J. 2014a, ApJ, 788, 81

Malo, L., Doyon, R., Feiden, G. A., Albert, L., Lafrenière, D., Artigau, É., Gagné, J., & Riedel, A. 2014b, ApJ, 792, 37

Mamajek, E. E. & Bell, C. P. M. 2014, MNRAS, 445, 2169

Mentuch, E., Brandeker, A., van Kerkwijk, M. H., Jayawardhana, R., & Hauschildt, P. H. 2008, ApJ, 689, 1127

Messina, S., Lanzafame, A. C., Feiden, G. A., Millward, M., Desidera, S., Buccino, A., Curtis, I., Jofré, E., Kehusmaa, P., Medhi, B. J., Monard, B., & Petrucci, R. 2016, A&A, 596, A29

Messina, S., Lanzafame, A. C., Malo, L., Desidera, S., Buccino, A., Zhang, L., Artemenko, S., Millward, M., & Hambsch, F. J. 2017, A&A, 607, A3

Miret-Roig, N., Galli, P. A. B., Brandner, W., Bouy, H., Barrado, D., Olivares, J., Antoja, T., Romero-Gómez, M., Figueras, F., & Lillo-Box, J. 2020, A&A, 642, A179

Morris, B. M. 2020, ApJ, 893, 67

Naylor, T. & Jeffries, R. D. 2006, MNRAS, 373, 1251

Palla, F., Randich, S., Pavlenko, Y. V., Flaccomio, E., & Pallavicini, R. 2007, ApJ, 659, L41

Pecaut, M. J. & Mamajek, E. E. 2013, ApJS, 208, 9

—. 2016, MNRAS, 461, 794

Plavchan, P., Barclay, T., Gagné, J., Gao, P., Cale, B., Matzko, W., Dragomir, D., Quinn, S., Feliz, D., Stassun, K., Crossfield, I. J. M., Berardo, D. A., Latham, D. W., Tieu, B., Anglada-Escudé, G., Ricker, G., Vanderspek, R., Seager, S., Winn, J. N., Jenkins, J. M., Rinehart, S., Krishnamurthy, A., Dynes, S., Doty, J., Adams, F., Afanasev, D. A., Beichman, C., Bottom, M., Bowler, B. P., Brinkworth, C., Brown, C. J., Cancino, A., Ciardi, D. R., Clampin, M., Clark, J. T., Collins, K., Davison, C., Foreman-Mackey, D., Furlan, E., Gaidos, E. J., Geneser, C., Giddens, F., Gilbert, E., Hall, R., Hellier, C., Henry, T., Horner, J., Howard, A. W., Huang, C., Huber, J., Kane, S. R., Kenworthy, M., Kielkopf, J., Kipping, D., Klenke, C., Kruse, E., Latouf, N., Lowrance, P., Mennesson, B., Mengel, M., Mills, S. M., Morton, T., Narita, N., Newton, E., Nishimoto, A., Okumura, J., Palle, E., Pepper, J., Quintana, E. V., Roberge, A., Roccatagliata, V., Schlieder, J. E., Tanner, A., Teske, J., Tinney, C. G., Vanderburg, A., von Braun, K., Walp, B., Wang, J., Wang, S. X., Weigand, D., White, R., Wittenmyer, R. A., Wright, D. J., Youngblood, A., Zhang, H., & Zilberman, P. 2020, Nature, 582, 497

Prada Moroni, P. G., Valle, G., Dell'Omodarme, M., & Degl'Innocenti, S. 2016, Astronomische Nachrichten, 337, 819

Richert, A. J. W., Getman, K. V., Feigelson, E. D., Kuhn, M. A., Broos, P. S., Povich, M. S., Bate, M. R., & Garmire, G. P. 2018, Monthly Notices of the Royal Astronomical Society, 477, 5191

Rousset, G., Lacombe, F., Puget, P., Hubin, N. N., Gendron, E., Fusco, T., Arsenault, R., Charton, J., Feautrier, P., Gigan, P., Kern, P. Y., Lagrange, A.-M., Madec, P.-Y., Mouillet, D., Rabaud, D., Rabou, P., Stadler, E., & Zins, G. 2003, in Society of Photo-Optical Instrumentation Engineers (SPIE) Conference Series, Vol. 4839, Adaptive Optical System Technologies II, ed. P. L. Wizinowich & D. Bonaccini, 140–149

Schneider, A. C., Shkolnik, E. L., Allers, K. N., Kraus, A. L., Liu, M. C., Weinberger, A. J., & Flagg, L. 2019, AJ, 157, 234

Service, M., Lu, J. R., Campbell, R., Sitarski, B. N., Ghez, A. M., & Anderson, J. 2016, Publications of the Astronomical Society of the Pacific, 128, 095004

Shan, Y., Yee, J. C., Bowler, B. P., Cieza, L. A., Montet, B. T., Cánovas, H., Liu, M. C., Close, L. M., Hinz, P. M., Males, J. R., Morzinski, K. M., Vaz, A., Bailey, V. P., Follette, K. B., & MagAO Team. 2017, ApJ, 846, 93

Shaviv, G. & Salpeter, E. E. 1973, ApJ, 184, 191

Shkolnik, E. L., Allers, K. N., Kraus, A. L., Liu, M. C., & Flagg, L. 2017, AJ, 154, 69

Skrutskie, M. F., Cutri, R. M., Stiening, R., Weinberg, M. D., Schneider, S., Carpenter, J. M., Beichman, C., Capps, R., Chester, T., Elias, J., Huchra, J., Liebert, J., Lonsdale, C., Monet, D. G., Price, S., Seitzer, P., Jarrett, T., Kirkpatrick, J. D., Gizis, J. E., Howard, E., Evans, T., Fowler, J., Fullmer, L., Hurt, R., Light, R., Kopan, E. L., Marsh, K. A., McCallon, H. L., Tam, R., Van Dyk, S., & Wheelock, S. 2006, AJ, 131, 1163

Soderblom, D. R., Jones, B. F., Balachandran, S., Stauffer, J. R., Duncan, D. K., Fedele, S. B., & Hudon, J. D. 1993, AJ, 106, 1059

Somers, G., Cao, L., & Pinsonneault, M. H. 2020, ApJ, 891, 29

Somers, G. & Pinsonneault, M. H. 2015, Monthly Notices of the Royal Astronomical Society, 449, 4131

Stahler, S. W. 1983, ApJ, 274, 822

Sullivan, K. & Kraus, A. L. 2021, ApJ, 912, 137

Terrien, R. C., Mahadevan, S., Deshpande, R., & Bender, C. F. 2015, ApJS, 220, 16

Winters, J. G., Henry, T. J., Jao, W.-C., Subasavage, J. P., Chatelain, J. P., Slatten, K., Riedel, A. R., Silverstein, M. L., & Payne, M. J. 2019, AJ, 157, 216

Wood, M. L., Mann, A. W., & Kraus, A. L. 2021, AJ, 162, 128

Yi, S., Demarque, P., Kim, Y.-C., Lee, Y.-W., Ree, C. H., Lejeune, T., & Barnes, S. 2001, ApJS, 136, 417

Ziegler, C., Law, N. M., Baranec, C., Morton, T., Riddle, R., De Lee, N., Huber, D., Mahadevan, S., & Pepper, J. 2018, AJ, 156, 259

Zúñiga-Fernández, S., Bayo, A., Elliott, P., Zamora, C., Corvalán, G., Haubois, X., Corral-Santana, J. M., Olofsson, J., Huélamo, N., Sterzik, M. F., Torres, C. A. O., Quast, G. R., & Melo, C. H. F. 2021, A&A, 645, A30

Zuckerman, B., Song, I., Bessell, M. S., & Webb, R. A. 2001, ApJ, 562, L87